Atelier commun A.S. Gaia - PNCG

Populations stellaires et modélisation de la Galaxie : maintenant et après Gaia, observations complémentaires au sol

SF2A 2010

24 juin 2010

Table des matières

Préface

Ce fascicule rassemble l'ensemble des textes publiés pour les présentations orales et les posters présentés lors de l'Atelier Commun AS Gaia – PNCG « **Populations stellaires et modélisation de la Galaxie: maintenant et après Gaia, observations complémentaires au sol** », qui s'est tenu le jeudi 24 juin à Marseille lors de la semaine de la SF2A 2010. Les présentations ou posters eux-mêmes sont disponibles à l'adresse suivante :
http://wwwhip.obspm.fr/AS/animation/article/journee-sf2a-2010.

Cette Session a fait suite à un atelier commun SF2A/SAIt/PNCG/PNPS/AS-Gaia « **Resolved Stellar Populations** » les 22 et 23 juin. Le programme de cet atelier est disponible à l'adresse suivante :
http://obswww.unige.ch/~corinne/SF2AMarseille2010/atelier10SF2SAI_pncg_pnps.htm.
Les textes individuels sont disponibles sur l'ADS et à l'adresse suivante :
http://sf2a.cesr.fr/php/spip/spip.php?article279#12

Ces deux sessions ont permis de rassembler une grande partie des scientifiques travaillant sur Gaia en France (analyse des données et préparation de l'exploitation scientifique) ainsi que des collègues des domaines de la Physique Stellaire et de la Physique des Galaxies travaillant sur les Populations Stellaires dans les galaxies résolues en étoiles et sur la modélisation de la Galaxie.

Les textes sont ici présentés dans l'ordre des présentations orales (présentations invitées et contributions), puis l'ordre alphabétique des posters. Les numéros des pages correspondent à la publication « Proceedings SF2A 2010, 21-24 June 2010, Marseille, France, S. Boissier, M. Heydari-Malayeri, R. Samadi & D. Valls-Gabaud (eds) », disponible à l'adresse suivante :
http://sf2a.cesr.fr/php/spip/spip.php?article279#2.

L'ensemble des publications des Journées de la SF2A 2010 sont disponibles individuellement sur l'ADS et à l'adresse suivante : http://sf2a.cesr.fr/2010/book.pdf.

La présentation de l'AS Gaia pendant la session plénière de la SF2A a porté sur la Galaxie et été donnée par Misha Haywood le jeudi 24 juin au matin : **Gaia : promises and expectations in the field of galactic astronomy**. La présentation est disponible en ligne :
http://wwwhip.obspm.fr/AS/squelettes/doc/Haywood_SF2A_ASGaia_2010.pdf

Catherine Turon et Frédéric Arenou

Atelier commun ASGaia - PNCG

Populations stellaires et modélisation de la Galaxie : maintenant et après Gaia, observations complémentaires au sol

SF2A 2010

24 juin 2010

Présentations invitées et contributions orales

14:00 - 14:30	**C. Reylé et al.**, The Besançon Galaxy model : comparisons to photometric surveys and modelling of the Galactic bulge and discs
14:30 - 14:45	**C. Worley et al.**, Tests of MATISSE on large spectral datasets from the ESO archive
14:45 - 15:15	**P. Bonifacio**, The chemical enrichment in the halo from first galactic stars
15:15 - 15:30	**S. Raimond et al.**, 3D tomography of local interstellar gas and dust
15:30 - 15:45	**L. Ciesla et al.**, SED fitting of nearby galaxies in the Herschel Reference Survey
15:45 - 16:15	Pause
16:15 - 16:45	**P. Jablonka**, The dynamical and chemical evolution of dwarf spheroidal galaxies
16:45 - 17:15	**B. Famaey & I. Minchev**, Dynamical modelling of the Galaxy and stellar migration in the disc

THE BESANÇON GALAXY MODEL: COMPARISONS TO PHOTOMETRIC SURVEYS AND MODELLING OF THE GALACTIC BULGE AND DISC

C. Reylé[1], A. C. Robin[1], M. Schultheis[1] and D.J. Marshall[2]

Abstract. Exploring the in-plane region of our Galaxy is an interesting but challenging quest, because of the complex structure and the highly variable extinction. We here analyse photometric near-infrared data using the Besançon Galaxy Model in order to investigate the shape of the disc and bulge. We present new constraints on the stellar disc, which is shown to be asymmetric, and on the bulge, which is found to contain two populations. We present how the Galaxy model is used in the framework of the preparation of the Gaia mission.

Keywords: stellar population model, bulge, disc, large scale survey, Gaia

1   Introduction

The population synthesis approach aims at assembling together current scenarii of galaxy formation and evolution, theory of stellar formation and evolution, models of stellar atmospheres and dynamical constraints, in order to make a consistent picture explaining currently available observations of different types (photometry, astrometry, spectroscopy) at different wavelengths. The validity of any Galactic model is always questionable, as it describes a smooth Galaxy, while inhomogeneities exist, either in the disc or the halo. The issue is not to make a perfect model that reproduces the known Galaxy at any scale. Rather one aims at producing a useful tool to compute the probable stellar content of large data sets and therefore to test the usefulness of such data to answer a given question in relation with Galactic structure and evolution. Modelling is also an effective way to test alternative scenarii of galaxy formation and evolution.

In section 2, we give a brief description of the model. In section 3 we describe recent and future analysis of near-infrared data with the model. In section 4 we describe the use of the model for the preparation of the Gaia mission.

2   The Besançon Galaxy model: ingredients and recipe

The main scheme of the model is to reproduce the stellar content of the Galaxy, using some physical assumptions and a scenario of formation and evolution. We essentially assume that stars belong to four main populations : the thin disc, the thick disc, the stellar halo, and the outer bulge. The modelling of each population is based on a set of evolutionary tracks, assumptions on density distributions, constrained either by dynamical considerations or by empirical data, and guided by a scenario of stellar formation and evolution, that is to say assumptions on the initial mass function (IMF) and the star formation rate (SFR) history for each population. The originality of the Besançon model, as compared to a few other population synthesis models presently available for the Galaxy, is the dynamical self-consistency. The Boltzmann equation allows the scale height of an isothermal and relaxed population to be constrained by its velocity dispersion and the Galactic potential (Bienaymé et al.1987). The use of this dynamical constraint avoids a set of free parameters and gives the model an improved physical credibility. More detailed descriptions on these constraints can be found in Robin et al. 2003. Simulations can be performed on-line.[*]

---

[1] Observatoire de Besançon, Institut Utinam, UMR CNRS 6213, BP 1615, 25010 Besançon Cedex, France

[2] Centre d'Etude Spatiale des Rayonnements, UMR 5187, 9, av du Colonel Roche, BP 44346, 31028 Toulouse Cedex 4, France
[*]`http://model.obs-besancon.fr`

Observational tests have been made in many directions in the optical, mostly at high latitudes, a few directions to magnitudes V=24-25 (Robin et al. 2000, Reylé & Robin 2001, Schultheis et al. 2006, Robin et al. 2008). An all-sky comparison has been made with the Guide Star Catalogue 2 (GSC2, see Fig. 1). The model has also been constrained using near-infrared data (Picaud & Robin, Reylé et al. 2009), X-ray data (Guillout et al. 1996), and UV (Todmal et al. 2010).
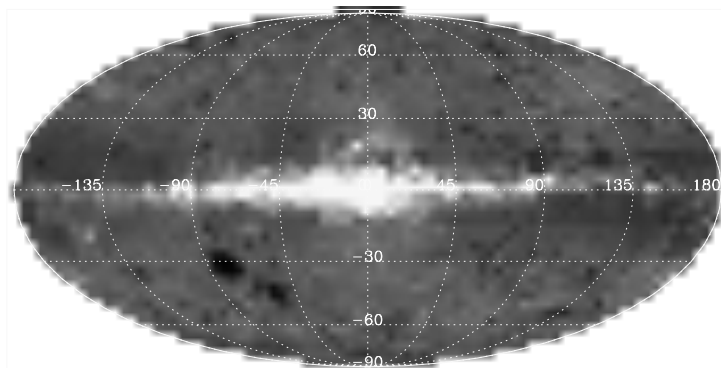
Fig. 1. Relative difference map, (model - GSC2)/GSC2, on a log scale, to magnitude V=17. The agreement is at 10% outside plane. Most of the discrepancy between the model and the observations are within of the Galactic plane, probably due to inadequate extinction in the plane (Drimmel et al. 2003).

3   Constraints on the external disc and central regions

The 2MASS survey is a powerful tool to study large scale structure in the Galaxy, particularly in the Galactic plane because NIR data are well suitable to study stellar populations in regions of medium to high extinction. A good estimate of the extinction is required to understand the structure in the Galactic plane. In the following studies, we used a three dimensional extinction map of the Galaxy (Marshall et al. 2006).

From the comparison of 2MASS star counts with the Besançon Galaxy model, we investigated the warp feature followed by stars (Reylé et al. 2009). We modelled the warp as a simple S-shape symmetrical but found that the warp is not symmetrical: the simple model reproduces well the northern side of the warp (positive longitudes), but not the southern side. The results also show that the stellar warp is less marked in stars than in the HI gas. Our result is well in agreement with studies in external galaxies, where van der Kruit (2007) noted that stellar discs look flatter than gas layers. This is understandable in a scheme where the HI warps start close to the truncation radius, truncation seen in the exponential distribution of stars which may be due to a threshold effect in the star formation efficiency.

Since the discovery of a triaxial structure in the Galactic central regions from COBE, numerous attempts have been done in order to characterize this structure and to investigate its origin. It is still unclear whether this structure had its origin from the early formation of the spheroid (as a typical bulge, similar to ellipsoidal galaxies) or was formed by a bar instability later in the disc. The question of formation history is crucial and necessary to investigate, as our Galaxy is a benchmark for understanding formation of disc galaxies. Thanks to the ability of the model to simulate the stellar populations as they are seen in surveys, we compared model simulations with 2MASS star counts in all the region covered by the outer bulge. We show evidence for two independent structures, a triaxial bulge and a long and narrow structure which angles are different (Fig. 2, Robin et al., in prep.). Further studies are needed to confirm these preliminary conclusions, in particular kinematical data, helpful in understanding the dynamics, especially to measure the rotation and velocity dispersions of these populations.

4   The Besançon Galaxy model for the preparation of the Gaia mission

Preparing the Gaia mission requires large efforts dedicated to simulations of the observations. Several simulators have been constructed, generating telemetry, images, or the final database. All these tools use a Universe Model containing essentially the astronomical sources to be seen by Gaia and their characteristics, as well as a Relativity model and a radiation model for estimating the potential damage to the CCDs. The stellar content
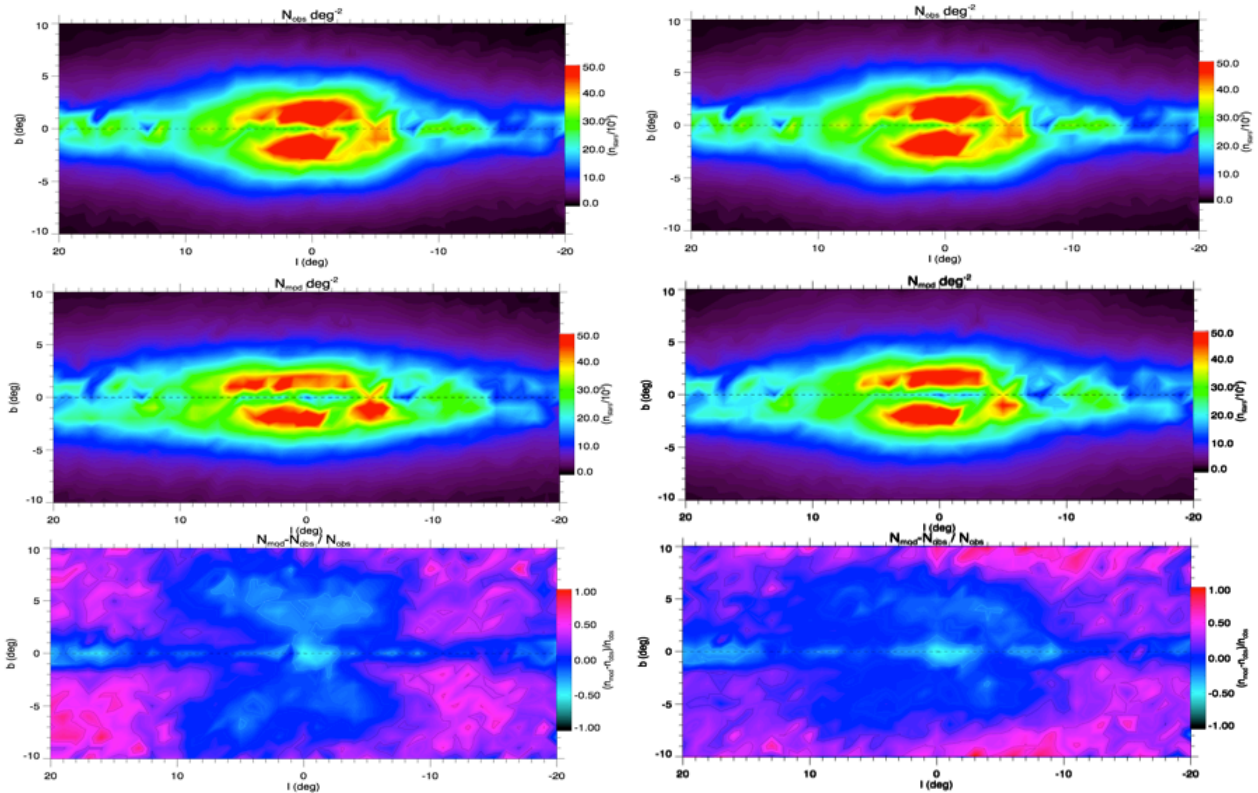
Fig. 2. Star counts up to magnitude K=12 from 2MASS data (top) compared with 2 models (middle panels) and residuals (Nmod-Nobs)/Nobs (bottom). Left: model with 1 bulge population. Right: model with 2 populations : a triaxial bulge and a thin elongated structure. In pink the excess in the model is at the level of 70%. The light blue corresponds to a lack in the model at the level of 50%. The 2-population model allows to nicely reproduce the boxy shape of the outer bulge region, while the 1-population model leaves significant X-shaped residuals. Near the Galactic center the nuclear bar population is missing in the model. The residuals in the outer region are not much significant due to the small number of stars in each bin.

of the Universe Model is simulated using the Besançon Galaxy model (Isasi et al. 2010). Fig. 3 shows the expected density of stars to magnitude G=20 as a function of galactic coordinates. The expected total number of stars is 1.3×10^9 (8.7×10^8 disc stars, 2.6×10^8 thick disc stars, 15×10^6 halo stars, and 10^8 bulge stars). Fig. 4 gives the expected number of stars as a function of spectral type and luminosity class. The right panel in Fig. 3 shows the expected density of stars in the (X,Y) plane, centered on the Sun. The sharp radius towards the anticenter is due to the cut-off radius of the thin disc at 14 kpc (from Ruphy et al. 1996). The Gaia data will bring a strong constraint on the shape and radius of the disc, as well as on many other parameters.

5   Conclusions

Population synthesis models are useful tools for data interpretation. Although imperfect they allow a better understanding of galactic structure and evolution, eases the interpretation, and is useful for the preparation of future surveys. Gaia will obtain distance, proper motions of more than 1 billion stars (about 1% of the Galaxy) as well as astrophysical parameters, radial velocities for about 250 million stars, and abundances for a few million stars. It will be a challenge to fit Gaia data with (simplistic) models! Since then, efforts have to been made to get stellar population models with self-consistent dynamical modelling.

References

Bienaymé, O., Robin, A. C., Crézé, M. 1987, A&A, 180, 94

Drimmel, R., Cabrera-Lavers, A., López-Corredoira, M. 2003, A&A, 409, 205
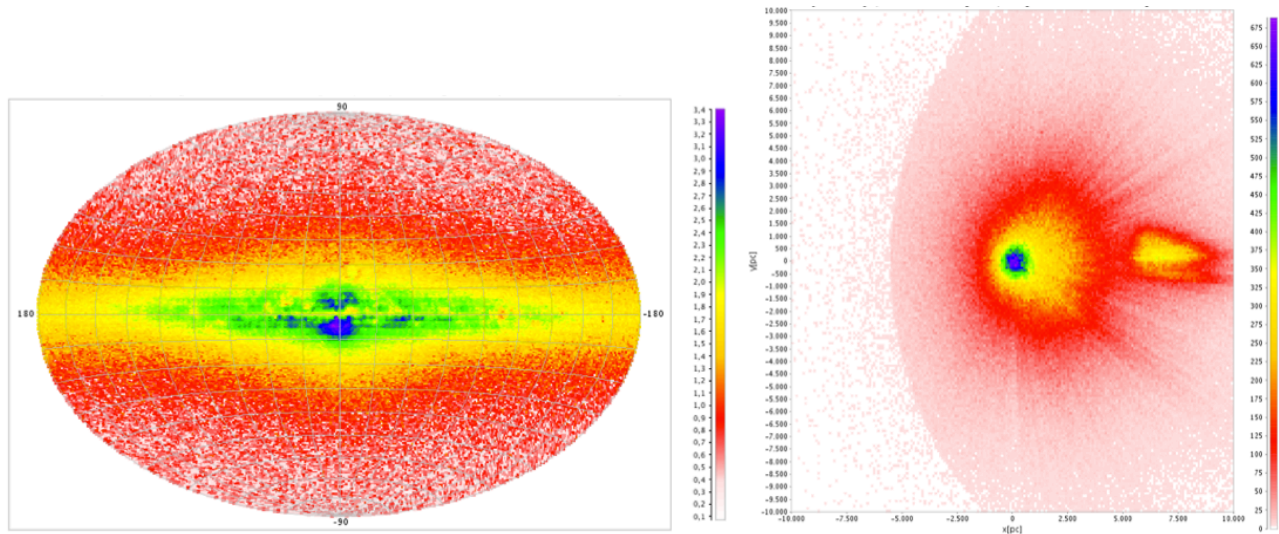
Fig. 3. Left: Expected total sky density (log of the number of objects per square degree) to magnitude G=20 from the Gaia Universe Model simulations (GUMS). Right: Expected total sky density in the X,Y plane, centered on the Sun.

spectralType	Total
O	3
B	3589
A	24916
F	296763
G	473337
K	349763
M	99937
L	1
Be	0
WR	0
AGB	9817
Other	1183
Total	1259309

lumClass	Total
BrightGiant	8812
Giant	173305
MainSequence	885651
Other	401
PreMainSequence	4584
SubGiant	185774
SuperGiant	18
WhiteDwarf	764
Total	1259309

Fig. 4. Expected number of stars $\times 10^{-3}$ at magnitude G=20 from the Gaia Universe Model simulations (GUMS).

Guillout, P., Haywood, M., Motch, C., Robin, A. C. 1996, A&A, 316, 89

Isasi, Y., Figueras, F., Luri, X., Robin, A. C. 2010, Highlights of Spanish Astrophysics V, 415

Marshall, D. J., Robin, A. C., Reylé, C., Schultheis, M., Picaud, S. 2006, A&A, 453, 635

Picaud, S., & Robin, A. C. 2004, A&A, 428, 891 bibitemReylé, C., Robin, A. C. 2001, A&A, 373, 886

Reylé, C., Marshall, D.J., Robin A.C., Schultheis, M. 2009, A&A 495, 819

Robin, A. C., Reylé, C., Crézé, M. 2000, A&A, 359, 103

Robin, A. C., Reylé, C., Derrière, S., Picaud, S. 2003. A&A, 409, 523 -540

Robin, A. C., Rich, R. M., Aussel, H. et al. 2007, ApJS, 172, 545

Ruphy, S., Robin, A.C., Epchtein, N., Copet, E., Bertin, E., Fouqué, P., Guglielmo, F. 1996, A&A, 313, L21

Schultheis, M., Robin, A. C., Reylé, C., McCracken, H. J., Bertin, E., Mellier, Y., Le Fèvre, O. 2006, A&A, 447, 185

Todmal, S.S, Gosh, S.K., Ojha, D.K., Robin, A.C. 2010, Bull. Astr. Soc. India, 1, 205

van der Kruit, P.C., 2008, in Formation and Evolution of Galaxy Disks, ASP Conference Series, Eds. J. G. Funes, S.J.,
    E. M. Corsini

THE MATISSE ANALYSIS OF LARGE SPECTRAL DATASETS FROM THE ESO ARCHIVE

C. Worley[1], P. de Laverny[1], A. Recio-Blanco[1], V. Hill[1], Y. Vernisse[1], C. Ordenovic[1] and A. Bijaoui[1]

Abstract. The automated stellar classification algorithm, MATISSE, has been developed at the Observatoire de la Côte d'Azur (OCA) in order to determine stellar temperatures, gravities and chemical abundances for large datasets of stellar spectra. The Gaia Data Processing and Analysis Consortium (DPAC) has selected MATISSE as one of the key programmes to be used in the analysis of the Gaia Radial Velocity Spectrometer (RVS) spectra. MATISSE is currently being used to analyse large datasets of spectra from the ESO archive with the primary goal of producing advanced data products to be made available in the ESO database via the Virtual Observatory. This is also an invaluable opportunity to identify and address issues that can be encountered with the analysis large samples of real spectra prior to the launch of Gaia in 2012. The analysis of the archived spectra of the FEROS spectrograph is currently underway and preliminary results are presented.

Keywords: stars:fundamental parameters, astronomical databases, methods: data analysis

1 Introduction

Galactic archæology is the study of large datasets of stellar spectra in the search for underlying structures and populations within the Galaxy. Identification of such structures and populations allows astronomers to test theories of galactic formation and evolution. The main tool that is created by the assimilation of this information is a kinematic and chemical chart of the Galaxy. This chart is contructed using the key stellar parameters of radial velocity, proper motion, distance, effective temperature, surface gravity, metallicity and chemical abundances.

The current and future generations of telescopes and instruments have, and will, create large spectral datasets over a wide range of resolutions, wavelengths and signal-to-noise (SNR). This wealth of data can be used to derive kinematic and chemical signatures for the observed stars, providing unprecedented detail of the surrounding Galaxy. The analysis of such large datasets cannot be carried out 'by hand' and so it is essential that automated stellar classification algorithms are developed in order to provide a consistent and efficient analysis of these data.

The Gaia satellite is at the forefront of astronomical technology and, once launched, it will observe approximately a billion stars in the Galaxy. For this sample Gaia will measure stellar distances to new precisions at milliarcsecond accuracies. Of the three instruments that Gaia will carry, the Radial Velocity Spectrometer (RVS) will observe spectra at two different resolutions (R∼11500 and R∼7000) over the wavelength domain from 847 nm to 874 nm. This wavelength region includes several key spectral features which will be used to determine the stellar parameters for at least 25 million stars.

Table 1. Details of the ESO spectrographs and publicly available archived spectra that are part of the AMBRE project.

Spectrograph	Resolution	Wavelength Range (nm)	No. Spectra
FEROS	48,000	$350 - 920$	$\sim 23,000$
HARPS	115,000	$378 - 691$	$\sim 40,000$
UVES	$40,000 - 110,000$	$300 - 1100$	$\sim 35,000$
Flames/GIRAFFE	$5,600 - 46,000$	$370 - 900$	$\sim 100,000$

2 The AMBRE project: tests of MATISSE

The stellar classification algorithm, MATISSE, is being developed at the Observatoire de la Côte d'Azur (OCA) (Recio-Blanco et al. 2006). It has been selected by the Gaia Data Processing Consortium (DPAC) as one of three stellar classification codes that will be used to analyse the RVS spectra for classification of the Gaia stellar sample. The AMBRE project team at OCA oversees the development of MATISSE and the work being carried out by AMBRE is formally connected to the Gaia DPAC under the Generalized Stellar Parametrizer-spectroscopy (GSP-spec) Top Level Work Package which is overseen by Coordination Unit 8 (CU8).

The AMBRE Project is the analysis of the archived spectra of four European Southern Observatory (ESO) spectrographs under a contract between ESO and OCA. The characteristics of the four spectrographs in question are listed in Table 1. The stellar parameters of effective temperature (T_{eff}), surface gravity (log g), metallicity ([M/H]), and α element abundances ([α/Fe]) will be derived for each of the archived stellar spectra. These will be delivered to ESO for inclusion in the ESO database and then made available to the astronomical community via the Virtual Observatory in order to encourage greater use of the archived spectra.

This analysis of the archived spectra of four separate instruments is a unique opportunity to test the performance of MATISSE on large datasets of real spectra. The datasets also include the Gaia RVS wavelength domain and resolutions and this will enable rigorous testing of MATISSE on general and Gaia-like spectra. This is necessary in order to optimise the performance of MATISSE in the Gaia analysis pipeline that is being compiled at the Centre National d'Etudes Spatiales (CNES). As such the AMBRE project has been formally designated as a sub-work package under GSP-spec.

3 MATISSE & FEROS

MATISSE (MATrix Inversion for Spectral SynthEsis) is an automated stellar classification algorithm based on a local multi-linear regression method. It derives stellar parameters ($\theta = T_{eff}$, log g, [M/H], individual chemical abundances) by the projection of an input observed spectrum on a vector $B_{\theta}(\lambda)$. The $B_{\theta}(\lambda)$ vector is an optimal linear combination of theoretical spectra calculated from a synthetic spectra grid. Key features in the observed spectrum due to a particular θ are reflected in the corresponding $B_{\theta}(\lambda)$ vector indicating the particular regions which are sensitive to θ (Recio-Blanco et al. 2006; Bijaoui et al. 2008).

A grid of high resolution synthetic spectra has been calculated using the MARCS stellar atmosphere models (Gustafsson et al. 2008) for $T_{eff} < 8000$ K. The grid spans the entire optical domain across the following stellar parameter range: $3{,}000$ K $< T_{eff} < 8{,}000$ K; $0.5 <$ log g < 5.0; $-5 <$ [M/H] $< +1$.
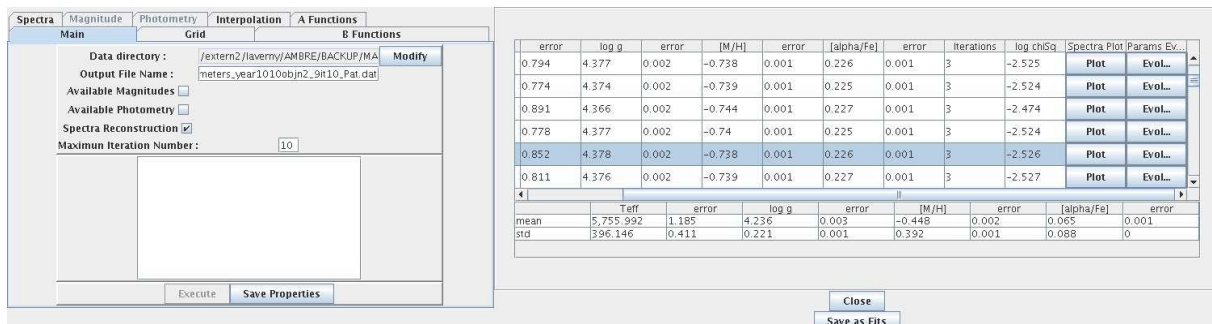
Fig. 1. Matisse java application showing input interface and results display.

MATISSE has been developed for integration into the CNES pipeline and also as a standalone java appli-
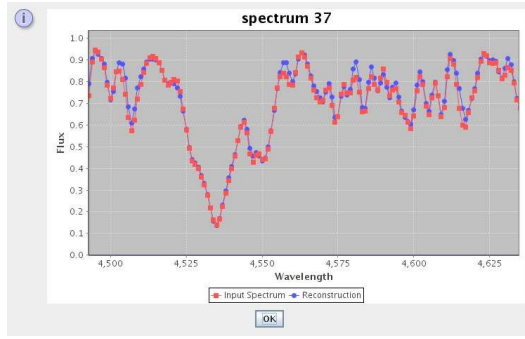
Fig. 2. Example of the comparison between the observed spectrum and the synthetic spectrum reconstructed at the stellar parameters of the corresponding MATISSE solution.
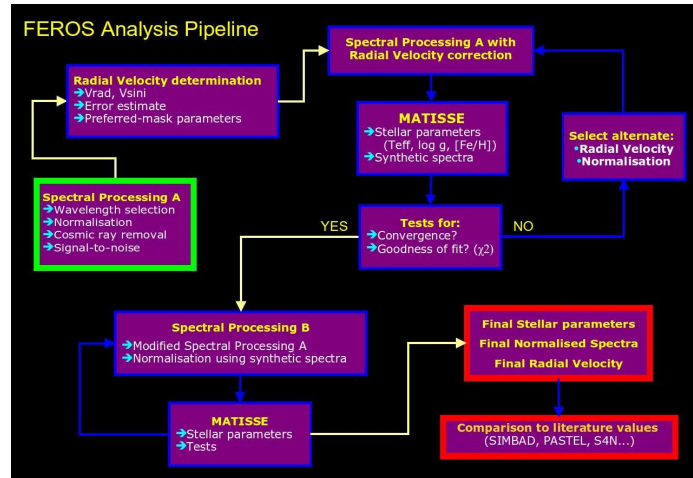
Fig. 3. Flowchart showing the different stages of analysis that the observed spectra undergoes in the FEROS analysis pipeline.

cation for use in a wide variety of projects. The archived spectra of the FEROS spectrograph (see Table 1) are currently being analysed using the java application. A picture of the java interface is shown in Figure 1. To the left is the user input where the observed spectra, signal-to-noise and photometric files can be specfied. To the right is the results display showing the parameters derived for the spectra as well as functions that enable the visual comparison of the observed spectrum with synthetic spectrum generated at the derived stellar parameters. An example of this is shown in Figure 2.

The java application can also be integrated into a local analysis pipeline, and such a pipeline has been developed for the FEROS spectra. Figure 3 shows a flowchart of the key stages of analysis in the FEROS pipeline. After initial normalisation and cleaning of the observed spectra the radial velocities are determined using a cross-correlation programme which compares the observed spectrum to masks created from synthetic spectra (private communication, C. Melo). A second stage of normalisation then occurs which includes the radial velocity correction to shift the spectra to laboratory wavelengths. The next stage is inital MATISSE analysis and the resulting stellar parameters are tested for convergence and for goodness of fit using a χ^2 test between the observed spectrum and the reconstructed synthetic spectrum. Potential issues regarding normalisation and radial velocity corrections are identified and remedied at this stage.

An iterative procedure is then executed which again cleans and normalises the observed spectrum but now normalisation is made relative to the reconstructed spectrum of the previous MATISSE analysis. This newly normalised spectrum is entered into MATISSE to derive new stellar parameters. This analysis cycle between normalisation and stellar parameter derivation is repeated ten times in order to converge on the final stellar parameters. Ultimately the procedure produces the final stellar parameters, the final normalised observed spectrum and the final reconstructed synthetic spectrum. This final observed normalised spectrum is entered into the radial velocity programme to confirm the radial velocity and determine the final radial velocity errors.

A crucial stage which is currently underway is the identification of previously analysed stars within the FEROS dataset. Key databases such as the S[4]N library (Allende Prieto et al. 2004) have been used to identify reference samples within the FEROS dataset in order to compare the results of MATISSE with previous studies. Figure 4a compares the radial velocities calculated in the AMBRE-FEROS pipeline with the reported S[4]N values. There is good agreement between the two sets of values.

Stellar parameters were determined for the S[4]N sample using the AMBRE-FEROS pipeline and the comparison of the derived effective temperatures (T_{eff}) of AMBRE-FEROS with the S[4]N values is shown in Figure 4b. There is good agreement between the two sets of T_{eff} values. Further investigation of other reference samples is also being pursued for a comprehensive comparison between MATISSE and other extended studies.

4   Conclusion

As part of the AMBRE Project we have developed a comprehensive analysis pipeline for the FEROS dataset that feeds the cleaned and normalised stellar spectra into MATISSE for derivation of the stellar parameters.

(a)   (b)
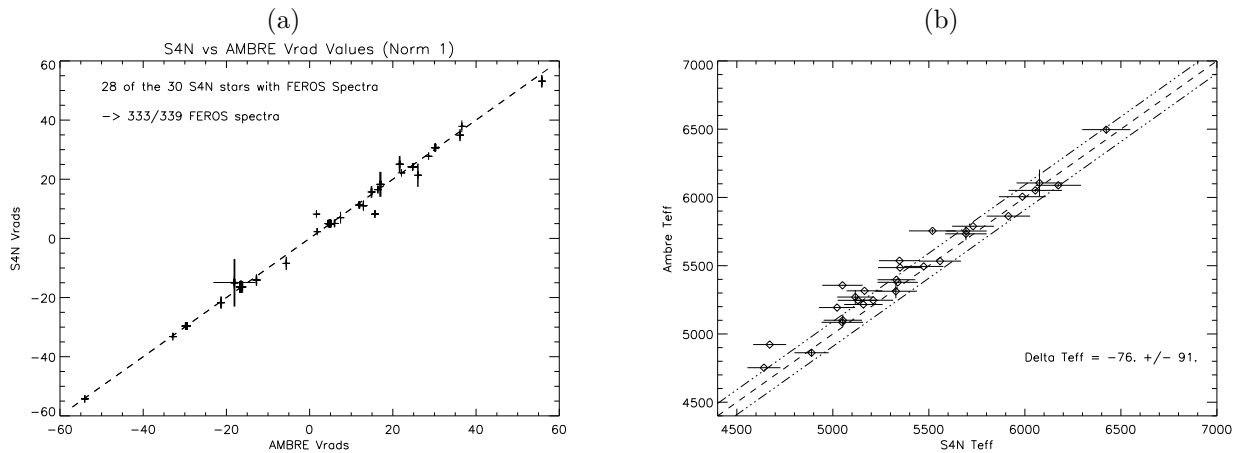
Fig. 4. a) Comparison of the radial velocity values reported in S^{4}N with those determined in the AMBRE-FEROS pipeline for the S^{4}N stars found in the FEROS dataset. Errorbars for each set are also shown. b) As for a) but for the effective temperature (T$_{eff}$).

This pipeline can be tailored to the specifications of the other three instruments that are also to be analysed in this project.

The preliminary results from the AMBRE-FEROS analysis show the great potential of MATISSE as a stellar classification tool for stand-alone projects and also for large-scale endeavours such as Gaia RVS spectra. The analysis of the ESO archive provides a unique opportunity to rigorously test MATISSE on RVS wavelengths and resolutions using large datasets of real stellar spectra in order to optimise its performance in the CNES pipeline.

The primary outcome of the AMBRE Project is to deliver to ESO the advanced data products (the stellar parameters) of the archived spectra for each of the four spectrographs, FEROS, UVES, HARPS and Flames/GIRAFFE. Considered as a whole this will be a homogeneous determination of stellar parameters for the archived spectra which will add an extra layer of key information to the ESO database. These parameters will in turn be made available to the astronomical community via the Virtual Observatory. The stellar parameters of these archived spectra will also create a galactic chemical chart which can be used to study stellar structures within the Milky Way in the pursuit of galactic archæology.

References

Allende Prieto, C., Barklem, P. S., Lambert, D. L., and Cunha, K.: 2004, A&A, 420, 183

Bijaoui, A., Recio-Blanco, A., and de Laverny, P.: 2008, in C. A. L. Bailer-Jones (ed.), American Institute of Physics Conference Series, Vol. 1082 of American Institute of Physics Conference Series, p 54-60

Gustafsson, B., Edvardsson, B., Eriksson, K., Jørgensen, U. G., Nordlund, Å., and Plez, B.: 2008, A&A, 486, 951

Recio-Blanco, A., Bijaoui, A., and de Laverny, P.: 2006, MNRAS, 370, 141

3D TOMOGRAPHY OF LOCAL INTERSTELLAR GAS AND DUST

S. Raimond[1], R. Lallement[1] and J-L. Vergely[2]

Abstract. Interstellar absorption data and Strömgren photometric data for target stars possessing a Hipparcos parallax have been combined to build a 3D tomography of local gas and dust. We show the latest inverted 3D distributions within 250 pc, compare gas and dust maps and discuss the present limitations and work in progress. Gaia extinction data and follow-up ground-based stellar spectra (e.g. with GYES at the CFHT) will provide a far larger database that should allow a 3D tomography of much higher quality and extended to much larger distances.

Keywords: galaxy: solar neighborhood, ISM: atoms, ISM: clouds

1 Introduction

The nearby interstellar medium plays several important roles in astrophysics. It is a tool for studying the evolution of the ISM, it provides the local conditions for photons and particles transport, it is a foreground which needs to be removed for studying specific objects, it is the ambient medium which governs limit conditions for a specific object and also the context environning such an object, etc. We present here studies of the gas and dust 3D distribution in the local interstellar medium (by local we mean here the interstellar medium within 250 pc).
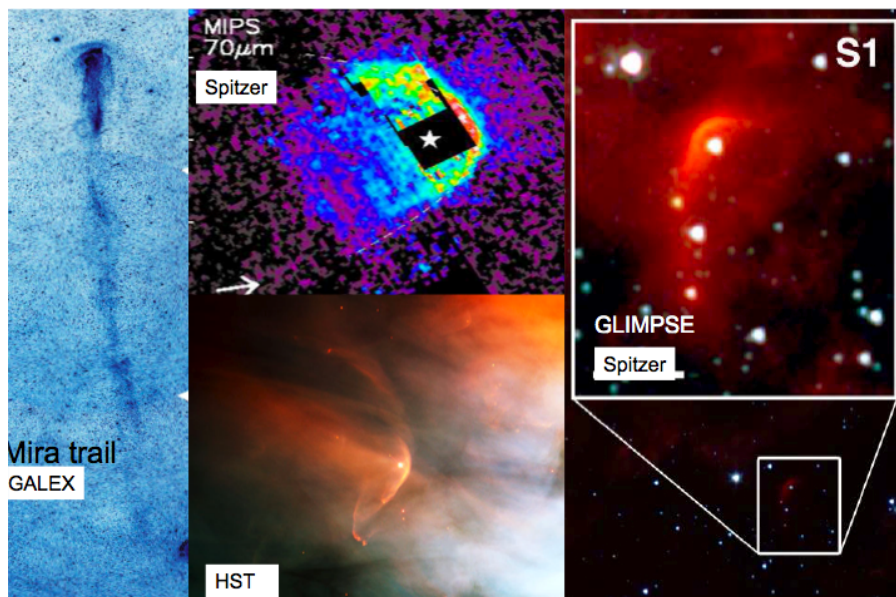
Fig. 1. Examples of interaction regions between stars and their surrounding environment. Stars collide the surrounding gas inducing a compression area. The knowledge of the ambient medium helps modeling the interaction.

---

[1] LATMOS, CNRS UMR 8190, 78280 Guyancourt, France

[2] ACRI-ST, 06904 Sophia Antipolis, France

2   Means of study

This work is based on NaI and CaII interstellar absorption lines in nearby star spectra and extinction obtained by Strömgren photometry. Both types of data can be inverted to get a 3D tomography of gas and dust. In addition, absorption lines assembled in an interstellar absorption database are a tool to distinguish between foreground absorption and local lines when studying objects by means of spectroscopy.

Fig. 2 illustrates an example of typical absorption lines.
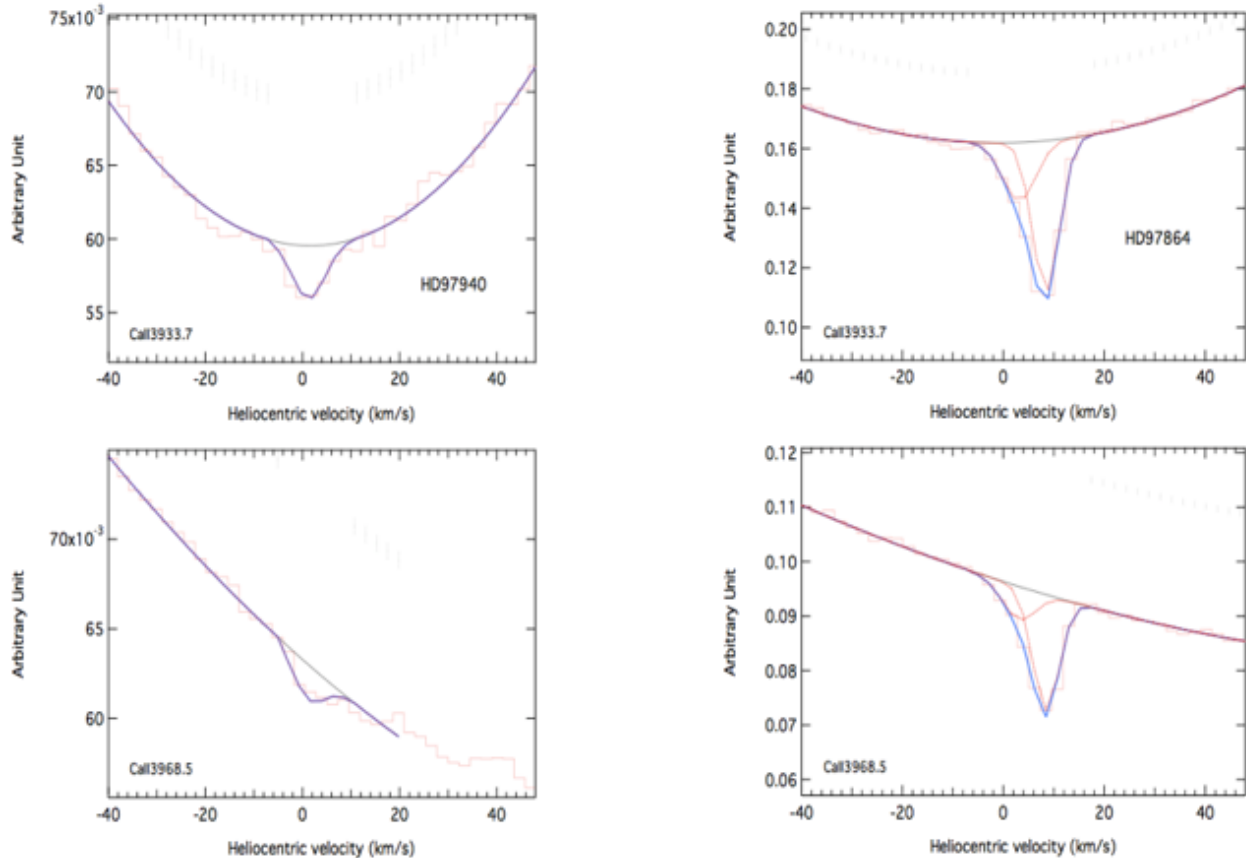
Fig. 2. Examples of CaII absorption lines of two stars in the same line of sight (the K line at 3934Å is on the top and the H line at 3968Å is on the bottom). On the left, HD97940 located at 85pc. A line is observed at about 2 km/s therefore a cloud begins before 85pc at this velocity. On the right, HD97864 located at 92pc. The same line is observed at about 2 km/s and a new one is detected around 9 km/s so the cloud beginning before 85pc is still present and another one at a velocity of about 9 km/s begins between 85 and 92pc.

3   Comparison of the different tracers

Gas and dust data can be combined with distances to the target stars to reconstruct by means of sophisticated inversion tools the gas and dust distributions in three dimensions. The obtained maps of the local interstellar medium reveal the so-called *Local Bubble*, a region devoid of dense gas that surrounds the Sun. Because of the difficulty to represent these distributions in three dimensions we show several cuts in the data cubes.

The different tracers are NaI, CaII and extinction. NaI is the tracer of dense and neutral gas, CaII is the tracer of dense neutral and also ionized gas and extinction locates the dust. We compare the results obtained with the different tracers in the meridian plane, i.e. the plane perpendicular to the galactic plane containing the Sun and the galactic center. These are shown in Fig. 3.

In all the cases, the Local Bubble surrounding the Sun is about 200pc wide in the galactic plane. This cavity is surrounded by large dense clouds: Ophiucus, Chamaeleon, Coalsack or Taurus. The maps reveal two

chimneys towards the halos and the cavity is tilted perpendicularly to the plane of the Gould Belt which is a ring of young stars and star forming regions tilted of about 20° towards the Galactic Center.

Within the Local Bubble neither NaI nor dust significant concentration is present, however it contains many diffuse clouds revealed in the CaII maps. These clouds are too ionized for being visible in NaI and too tenuous to be visible in extinction but they are detected thanks to CaII which traces the ionized gas.

The maps present strong similarities but also differences that may reflect gas states but also poor precision due to the limited amount of stars available for the inversion. Two articles are based on these maps, one compairing NaI and CaII (Welsh et al. 2010) and the other compairing NaI and extinction (Vergely et al. 2010).
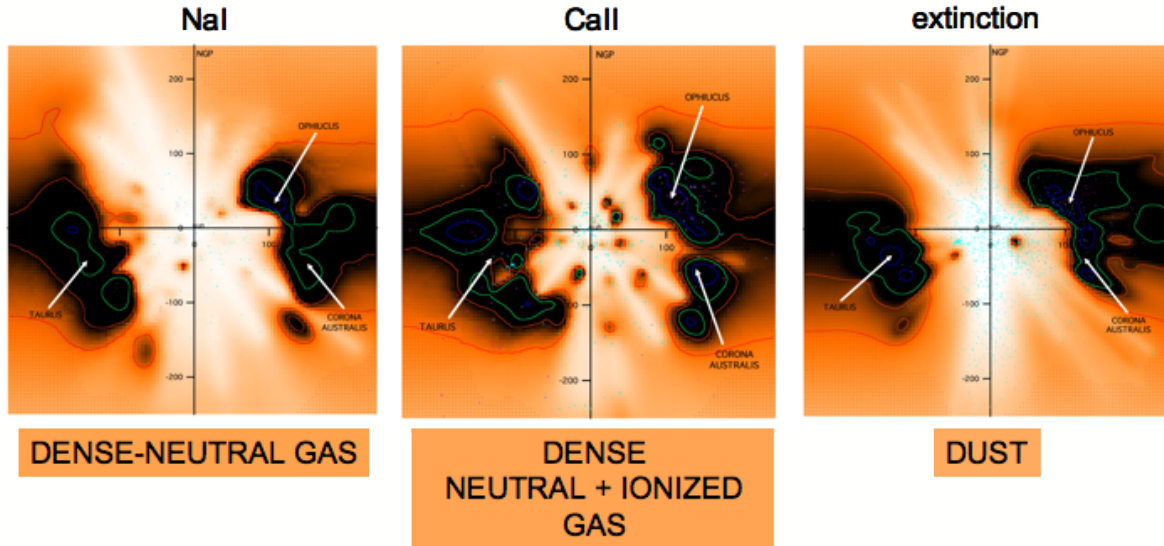
Fig. 3. Comparison of the local interstellar medium in the meridian plane. In each cut, the Galactic Center is on the right and the North Galactic Pole is on the top. Black indicates an important density whereas white represents diffuse regions. On the left, the map with NaI. On the middle, the map with CaII. On the right, the map with extinction.

4 Comparison between integrated gas and dust

In Fig. 4 neutral gas (on the left) and dust (on the middle) integrated back within the 3D cubes between the Sun and 200 pc are represented in aitoff projection. Important similarities are visible between the total columns of neutral gas traced by neutral sodium and dust opacities. On the right of Fig. 4, dotted lines representing integrated dust until 200pc are superimposed on the map showing the dust emission integrated to infinity derived from infrared data (Finkbeiner et al. 1999). Firstly, isocontours correspond very well with the map, showing that the inversion method is robust in spite of the limited amount of stars. Secondly, since the isocontours are well matching the map at moderate and high latitude, this means that the majority of the dust observed on the map of Finkbeiner et al. 1999 is located within 200pc.
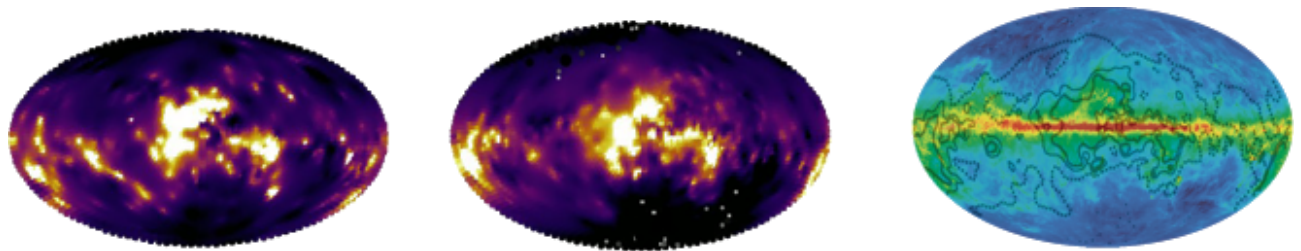
Fig. 4. Neutral gas (on the left) and dust (on the middle) integrated between the Sun and 200pc. On the right, map of the total column of dust, i.e. integrated to infinity (Finkbeiner et al. 1999). Dotted lines representing integrated dust until 200pc are superimposed.

5   Determination of the distance towards nearby structures

One of the interests of these inversions is the possibility to identify nearby structures seen in 2D maps and obtain an information on their distance, based on the kinematics. In particular, some clouds seen in the 21 cm HI data maps from the LAB Survey (Kalberla et al. 2005) are studied by compairing HI emission and NaI absorption velocities of the stars belonging to the database in the direction of the clouds. An example is presented in Fig. 5.

The map on the left in Fig. 5 presents a structure seen in HI emission between -10 and 0 km/s LSR. In order to define its distance, all the stars in this region are superimposed on the map and for each of them, we note the distance of the star and whether or not NaI is observed in absorption in this velocity interval.

We remark in this example that until 75pc, the stars don't present NaI absorption on their line of sight whereas from 75pc, all of them present NaI absorption lines around -3 km/s LSR. This means that the structure at -3 km/s LSR begins at around 75pc .

The spectra of the top and of the bottom of Fig. 5 illustrate respectively the NaI absorption spectrum of a star more distant than 75pc in the region and the HI emission spectrum in the same direction. This is an example showing that gas in the structure has a velocity around -3 km/s LSR. It would be the same with the NaI absorption and HI emission spectra of each star more distant than 75pc.

The cut on the right in Fig. 5 shows the structure seen in the same sky region in the NaI cube. It begins at 75pc, which is consistent with the distance found previously from the kinematics and allows the identification. Indeed, by using two methods based on different data, the first being the localization by velocity criteria and the second being the localization in the NaI cube only by absorption growth with distance criteria, the same result is obtained.

This identified region corresponds to the high latitude molecular clouds known as MBM53, MBM54 and MBM55 (Magnani et al. 1985). (Magnani et al. mapped the sky looking for high latitude clouds emitting CO and named them MBM.) Their initial estimated distance was 150pc (Welty et al. 1989). At that time, the stars did not have Hipparcos parallax, so the distance of the cloud was badly estimated. Here we have improved the localization of the structure and shown that it is much closer than previously thought.

This analysis is currently extended to other dense clouds by comparing the NaI interstellar absorptions and the HI emission and by searching the clouds in the data cubes.
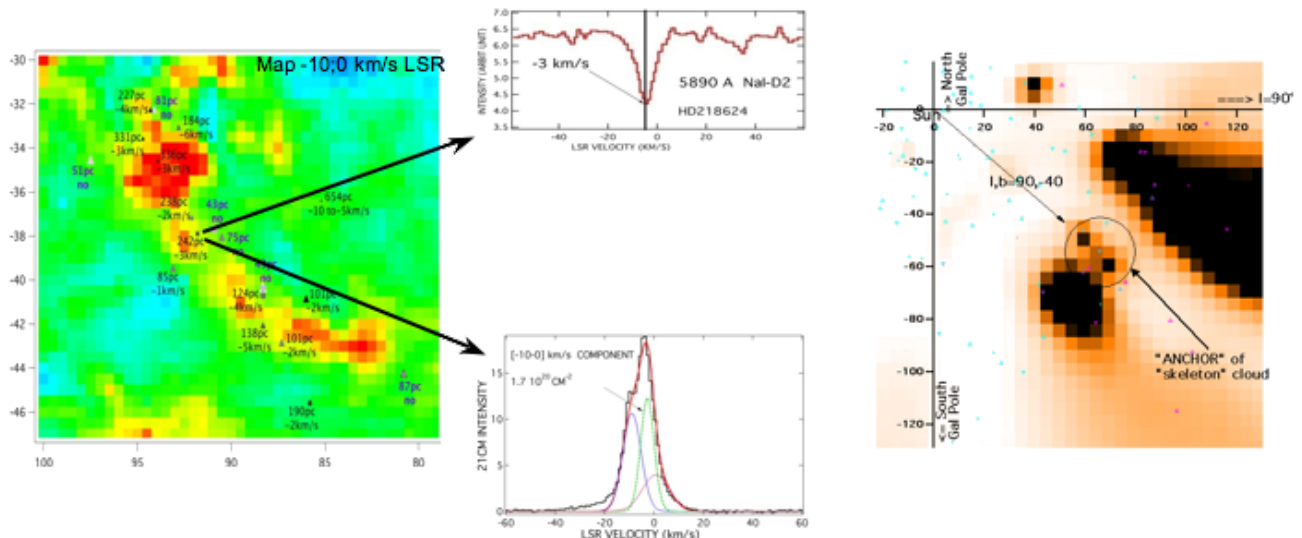
Fig. 5. Determination of the distance of a structure located at $l = 90°$ and $b = -40°$. On the left, the structure seen in HI emission in the velocity interval between -10 and 0 km/s LSR. On the top, NaI absorption spectrum of one of the stars more distant than the cloud with an absorption velocity around -3 km/s LSR. On the bottom, HI emission spectrum in the same direction with one of the peak around -3 km/s LSR. On the right, cut in the NaI cube at the good coordinates. The structure is visible and begins at 75pc.

6 Perspectives

Tomographic methods applied to local ISM dust and gas have been tested and validated on the current available absorption and extinction databases. In order to improve the accuracy and spatial resolution of the 3D maps, it is mandatory to increase the stellar databases, and have access to corresponding reliable parallaxes for the target stars. The GAIA mission and follow-up ground-based spectroscopic data with GYES will provide such considerably larger and better data sets. Combinations of the 3D distributions with 2D spectral maps should in addition allow to replace the roughly spherical clouds obtained by inversion by more realistic shapes.

References

Welsh, B. Y., Lallement, R., Vergely, J-L., Raimond, S. 2010, A&A, 510, 54

Vergely, J-L., Valette, B., Lallement, R., Raimond, S. 2010, A&A in press

Finkbeiner, D. P., Davis, M., Schlegel, D. J. 1999, ApJ, 524, 867

Kalberla, P.M.W., Burton, W.B., Hartmann, D., Arnal, E.M., Bajaja, E., Morras, R., Pöppel, W.G.L. 2005, A&A, 440, 775

Magnani, L., Blitz, L., Mundy, L. 1985, ApJ, 295, 402

Welty, D. E., Hobbs, L. M., Penprase, B.E., Blitz, L. 1989, ApJ, 346, 232

SED FITTING OF NEARBY GALAXIES IN THE HERSCHEL REFERENCE SURVEY

L. Ciesla[1], A. Boselli[1], V. Buat[1], L. Cortese[2], R. Auld[2], M. Baes[2], G.J. Bendo[2], S. Bianchi[2], J. Bock[2], D.J. Bomans[2], M. Bradford[2], N. Castro-Rodriguez[2], P. Chanial[2], S. Charlot[2], M. Clemens[2], D. Clements[2], E. Corbell[2], A. Cooray[2], D. Cormie[2], A. Dariush[2], J. Davies[2], I. De Looze[2], S. di Serego Alighieri[2], E. Dwek[2], S. Eales2, D. Elbaz[2], D. Fadda[2], J. Fritz[2], M. Galametz[2], F. Galliano[2], D.A. Garcia-Appadoo[2], G. Gavazzi[2], W. Gear[2], C. Giovanardi[2], J. Glenn[2], H. Gomez[2], M. Griffin[2], M. Grossi[2], S. Hony[2], T.M. Hughes[2], L. Hunt[2], K. Isaak[2], A. Jones[2], L. Levenson[2], N. Lu[2], S.C. Madden[2], B. O'Halloran[2] , K. Okumura[2], S. Oliver[2], M. Page[2], P. Panuzzo[2], A. Papageorgiou[2], T. Parkin[2], I. Perez-Fournon[2], D. Pierini[2], M. Pohlen[2], N. Rangwala[2], E. Rigby[2], H. Roussel[2], A. Rykala[2], S. Sabatini[2], N. Sacchi[2], M. Sauvage[2], B. Schulz[2], M. Schirm[2], M.W.L. Smith[2], L. Spinoglio[2], J. Stevens[2], S. Sundar[2], M. Symeonidis[2], M. Trichas[2], M. Vaccari[2], J. Verstappen[2], L. Vigroux[2], C. Vlahakis[2], C. Wilson[2], H. Wozniak[2], G. Wright[2], E.M. Xilouris[2], W. Zeilinger[2] and S. Zibetti [2]

Abstract. We compute UV to radio continuum spectral energy distributions of 51 nearby galaxies recently observed with SPIRE onboard Herschel and present infrared colours (in the $25 - 500\mu$m spectral range). SPIRE data of normal galaxies are well reproduced with a modified black body (β=2) of temperature $T \simeq$ 20 K. In ellipticals hosting a radio galaxy, the far-infrared (FIR) emission is dominated by the synchrotron nuclear emission. The colour temperature of the cold dust is higher in quiescent E-S0a than in star-forming systems probably because of the different nature of their dust heating sources (evolved stellar populations, X-ray, fast electrons) and dust grain properties.

Keywords: galaxies: ISM, spiral, elliptical and lenticular, infrared: galaxies

1   Introduction

By constructing the spectral energy distribution (SED) of any extragalactic source, its energetic output can be determined. The stellar component emits from the UV to near-infrared (NIR) domain, young and massive stars dominating the UV and old stars the NIR. Dust, produced by the aggregation of metals injected into the interstellar medium (ISM) by massive stars through stellar winds and supernovae, efficiently absorbs the stellar light, in particular that at short wavelengths, and re-emits it in the infrared domain (5μm-1mm). At longer wavelengths, the emission of normal galaxies is generally dominated by the loss of energy of relativistic electrons accelerated in supernovae remnants (Lequeux 1971; Kennicutt 1983) (synchrotron emission). SEDs are crucial for quantifying dust extinction and reconstructing the intrinsic distribution of the different stellar populations within galaxies. In particular, the importance of the infrared domain explored by Herschel resides in the dust that, by means of the absorption and scattering of UV, optical and NIR photons, modifies the stellar spectra of galaxies. The interpretation of the infrared SEDs of normal galaxies has already been the subject of several studies (e.g. Dale et al. 2007; Chary & Elbaz 2001) even within the Virgo cluster region (Boselli et al. 1998; 2003) which were limited in the infrared domain to $\lambda \leq 170$ μm (domain covered by ISO or Spitzer) With the Herschel data, we can extend to the sub-mm domain ($\lambda \leq 500$ μm) where the emission is dominated by the coldest dust component. This domain is crucial for determining galaxy properties such as the total mass of dust, and an accurate total infrared luminosity. Galaxies analysed in this work were observed

---

during the Herschel (Pilbratt et al. 2010) SPIRE (Griffin et al. 2010) science demonstration phase mainly as part of the Herschel Reference Survey (HRS), a guaranteed time key project designed to observe with SPIRE a volume-limited, K-band-selected, complete sample of nearby galaxies (Boselli et al. 2010), and the Herschel Virgo Cluster Survey (HeViCS), an open time key project focused on covering 60 sq.deg. of the Virgo cluster with PACS and SPIRE (Davies et al. 2010). The results of this analysis have been presented in Boselli et al. (2010b).

2   Far infrared colours

We determine the IR colours of the galaxies in order to quantify their spectral properties combining SPIRE and IRAS flux densities (Fig. 1). These colour diagrams indicate that in star-forming galaxies the flux density ratios $f60/f500$, $f25/f250$, or $f100/f250$ are strongly correlated with the generally used IRAS colour index $f60/f100$ (panels a, b and c). However, the dynamic range covered by $f60/f500$ is a factor of about 30 larger than that covered by the $f60/f100$ flux density ratio. The colour index is thus a powerful tracer of the average temperature of the dust component. Starburst galaxies, generally defined to have $f60/f100 > 0.5$ (Rowan-Robinson & Crawford 1989), show $f60/f500$ spanning from ~ 3 to ~ 30 and Sa-Sb have $f60/f500$ colours generally colder than Sbc-Scd, Sd, Im, BCD, and Irr. Early-types with a synchrotron-dominated IR emission (M87, M84) are well separated in all colour diagrams with respect to the other dust-dominated E-S0a. Therefore, we can use colour diagrams in order to identify and discriminate radio galaxies from the remaining early-types. The remaining early-types have colour indices indicating that the cold dust temperature is higher than in star-forming systems.
Figure 1 also shows that, despite possible uncertainties in the absolute flux calibration (15 %), the empirical SEDs of Dale & Helou (2002), Chary & Elbaz (2001), and Boselli et al. (2003), cover only qualitatively the wide range of infrared colours observed in our sample (even excluding the radio galaxies M87 and M84), underpredict the $f250/f350$ ratio for a given $f100/f250$ ratio (d), and do not reproduce the coldest colour temperatures observed in the diagram $f350/f500$ versus $f250/f350$ (f).

3   Spectral Energy Distribution

As a representative example of the target galaxies, we show the SED of two late-type galaxies (Fig2), M100 (NGC4321) and NGC4438, and two ellipticals (Fig3), M87 (NGC486) and M86 (NGC4406). The SED has been computed by combining data available in the literature. We match the 100μm IRAS data with a modified black body (β=2) of temperature $T \simeq 20$ K (magenta dashed line) and the radio data with a power law. Despite their very different morphology (M100 is a normal spiral galaxy while NGC4438 is a strongly interacting system), these two objects have quite similar SEDs. Contrarily, the galaxies M87 and M86 are both bright ellipticals but characterized by very different SEDs. In M87, the submilimeter emission detected by Herschel is due to synchrotron (Baes et al. 2010), while in M86 it is due to the cold dust nearly falling into the galaxy after its interaction with nearby companions (Gomez et al. 2010). These different SEDs for galaxies of the same morphological type clearly explain why galaxies of a given type have so different infrared colours.

4   Conclusions

The infrared colour index $f60/f500$ is more capable of detecting a starburst than $f60/f100$ due to a larger dynamical range. Normal galaxies show a gradual increase in their dust temperature along the Hubble sequence, from Sa to Sc-Im-BCD with the exception of E-S0a, where the dust temperature is higher than in star-forming systems probably because of the different nature of their dust heating sources. SPIRE colours can be used to discriminate thermal from synchrotron emission in radio galaxies. SED of radio galaxies clearly show the far-infrared dominated by the synchrotron emission. In normal galaxies, the modified black body seems to well reproduce the SPIRE data but it has to be detailed with a proper fit using the CIGALE code (Code Investigating GALaxy Emission, Noll et al. 2009).

References

Baes, M. et al. 2010, ApJ, 652, 283
Bendo, G. et al. 2010, A&A, 518, L65
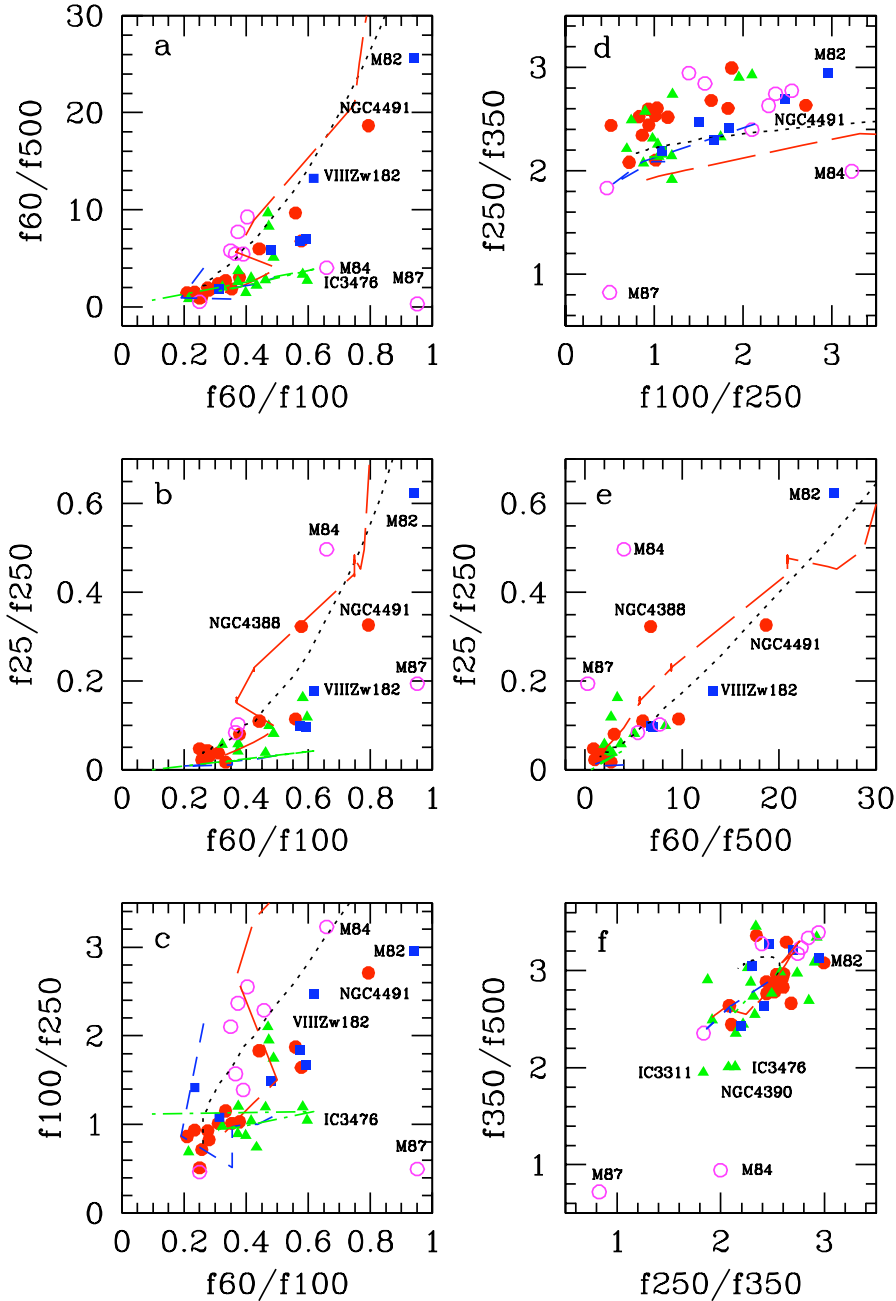
Fig. 1. The infrared colours of our targets. Galaxies are coded according to their morphological type: magenta empty circles for E-S0a, red filled circles for Sa-Sb, green triangles for Sbc- Scd, blue squares for Sd, Im, BCD, and Irr galaxies. The black dotted line indicates the colour expected from the Dale & Helou (2002) empirical SED, the red long-dashed line those from Chary & Elbaz (2001), the blue-short dashed, and the green dashed-dotted line the colours of the morphology- and luminosity-dependent templates of Boselli et al. (2003).

Boselli, A. and Gavazzi, G. 2006, PASP, 118, 517

Boselli, A., Lequeux, J., Sauvage, M., et al. 1998, A&A, 335, 53

Boselli, A., Gavazzi, G., Donas, J., Scodeggio, M. 2001, AJ, 121, 753

Boselli, A., Gavazzi, G., Sanvito, G., 2003, A&A, 402, 37

Boselli, A., Cortese, L., Deharveng, JM., et al. 2005, ApJ, 629, L29

Boselli, A., Boissier, S., Cortese, L., Buat, V., Hughes, T., Gavazzi, G. 2009, ApJ, 706, 1527

Boselli, A., Eales, S., Cortese, L., et al. 2010, PASP, 122, 261
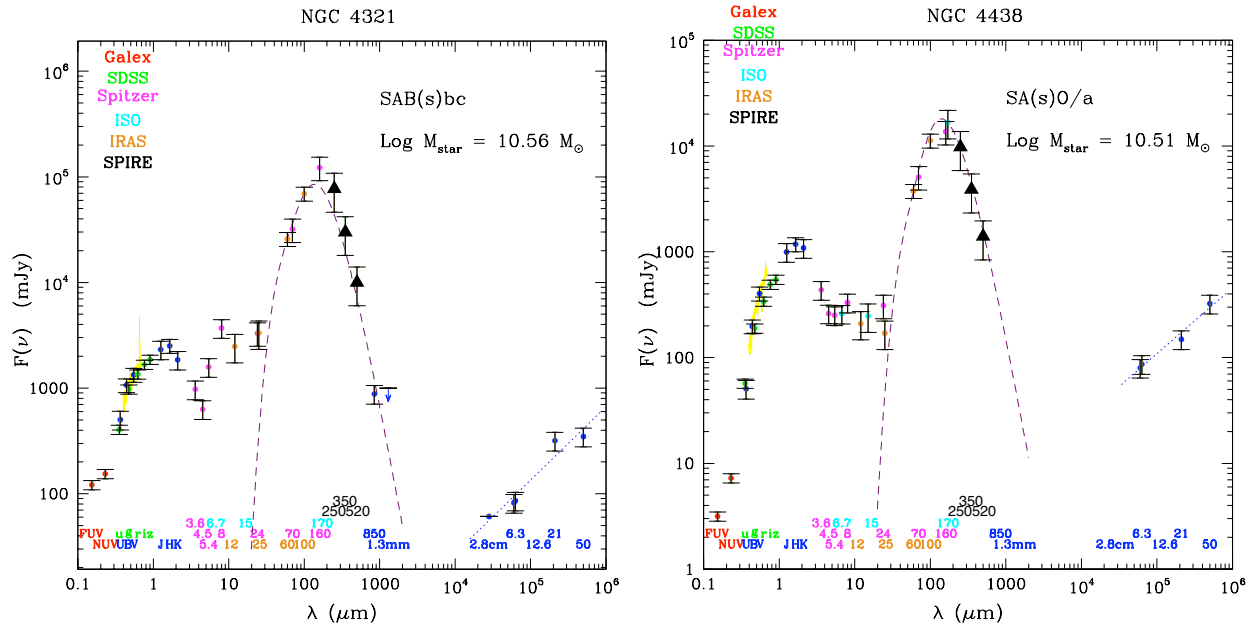
Fig. 2. The UV to radio SED of M100 (NGC4321) and NGC4438. Points are coloured according to the origin of the data. Black triangles are for Herschel-SPIRE data, red dots for GALEX data, green dots for SDSS data, magenta for Spitzer-IRAC and MIPS data, orange dots for IRAS data. Blue dots correspond to data from NED. The magenta dashed line shows a modified black body (β=2) of temperature $T \simeq 20$ K matching the 100μm IRAS data, while the blue dotted-line indicates the radio power law spectrum due to synchrotron emission. We fit the radio data with a power law (blue dotted-line).
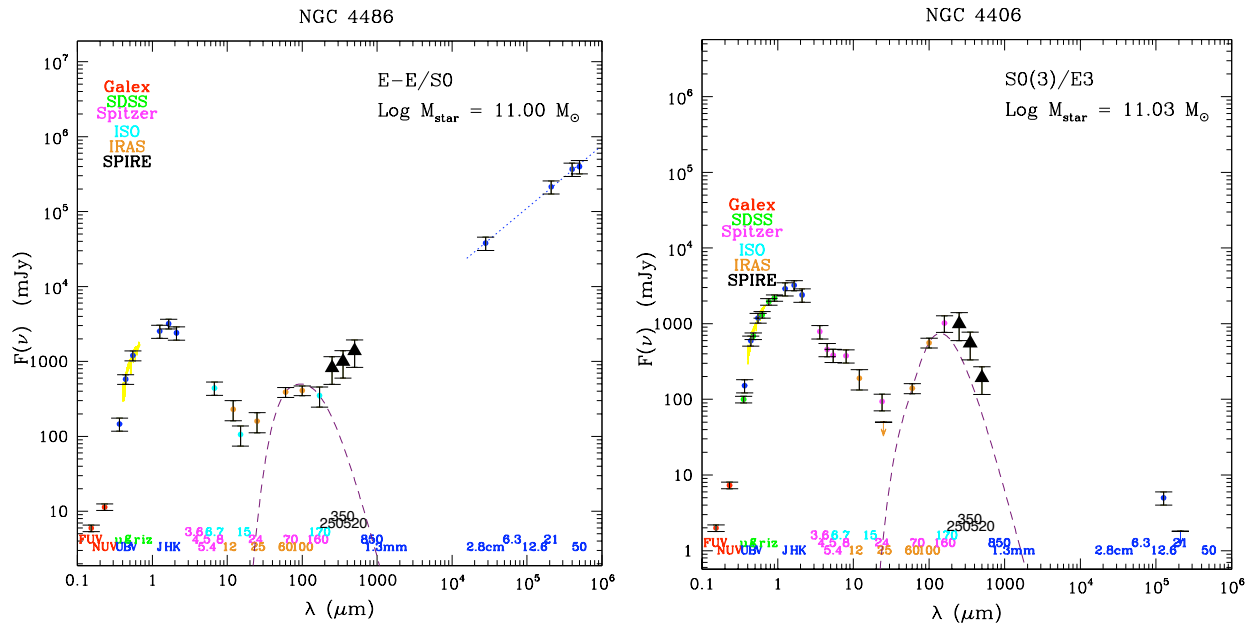
Fig. 3. The UV to radio SED of M87 (NGC4486) and M86 (NGC4406). Points are coloured according to the origin of the data. Black triangles are for Herschel-SPIRE data, red dots for GALEX data, green dots for SDSS data, magenta for Spitzer-IRAC and MIPS data, orange dots for IRAS data. Blue dots correspond to data from NED. The magenta dashed line shows a modified black body (β=2) of temperature $T \simeq 20$ K matching the 100μm IRAS data while the blue dotted-line indicates the radio power law spectrum due to synchrotron emission.

Boselli, A., Ciesla, L., Buat, V., et al. 2010, A&A, 518, L61

Chary, R. and Elbaz, D. 2001, ApJ, 556, 562

Cortese, L., Davies, J., Pohlen, M., et al. 2010, A&A, 518, L63

Dale, D., Gil de Paz, A., Gordon, K., et al. 2007, ApJ, 655, 863

Dale, D. & Helou, G. 2002, ApJ, 576, 159

Davies, J., Baes, M., Bendo, G., et al. 2010, A&A, 518, L48

Draine, B. and Li, A. 2007, ApJ, 657, 810

Draine, B., Dale, D., Bendo, G., et al. 2007, ApJ, 663, 866

Galliano, F., Madden, S., Jones, A., Wilson, C., Bernard, J. 2005, A&A, 434, 867

Gavazzi, G., Boselli, A., Donati, A., Franzetti, P., Scodeggio, M. 2003, A&A, 400, 451

Gomez, H. et al. 2010, A&A, 518, L45

Griffin, M., et al. 2010, A&A, 518, L3

Kennicutt, R. 1983, A&A, 120, 219

Lequeux, J. 1971, A&A, 15, 42

Noll, S., Burgarella, D., Giovannoli, E., Buat, V. et al. 2009, A&A, 507, 1793

O'Connell, R. 1999, A&A, 37, 603

Pilbratt, G., et al. 2010, A&A, 518, L1

Pohlen, M., et al. 2010, A&A, 518, L72

Rowan-Robinson, M., Crawford, J. 1989, MNRAS, 238, 523

Swinyard, B., Ade, P, Baluteau, J.P., et al. 2010, A&A, 518, L4

Wolfire, M., Hollenbach, D., McKee, C., Tielens, A., Bakes, E. 1995, ApJ, 443, 152

DYNAMICAL MODELING OF THE GALAXY
AND STELLAR MIGRATION IN THE DISK

B. Famaey[1] and I. Minchev[2]

Abstract. We exhibit the local and global effects of the non-axisymmetry of the Milky Way potential. In addition to creating moving groups in the Solar neighborhood, we show that spiral structure interacting with a central bar is an effective mechanism for mixing the whole stellar disk radially. This spiral-bar resonance overlap mechanism accounts for the absence of age-metallicity relation in the solar neighborhood, can create extended disks in both Milky Way-mass and low-mass galaxies, and could also be responsible for the formation of a thick disk component early-on in the Galaxy evolution.

Keywords: galaxy: kinematics and dynamics, galaxy: evolution

1 Introduction

Our Milky Way Galaxy is a unique laboratory in which to study galactic structure and evolution. The story of the efforts to obtain stellar kinematic data nicely illustrates how theoretical progress and data acquisition have to go hand in hand if one wants to gain insight into the structure and history of the Galaxy. Until recently, most observational studies have been limited to the solar neighbourhood. The zeroth order approximation for modelling these kinematic data assumes an axisymmetric model, in which the Local Standard of Rest is on a perfectly circular orbit. However, the local velocity field in the solar neighbourhood already displays signatures of the non-axisymmetry of the Galactic potential in the form of stellar moving groups containing stars of very different ages and chemical compositions (Famaey et al. 2005, 2007, 2008), the most prominent being the Hyades stream, the Sirius stream, and the Hercules stream (see Fig. 1 left panel). Here we investigate how to reproduce these streams with a bar and a spiral pattern, and how the combined effect of the bar and the spiral can cause radial migrations in the disk. Future astrometric and spectroscopic surveys will allow radical progress in our understanding of these effects of the non-axisymmetry of the Galactic potential.

2 Moving groups

Kalnajs (1991) suggested that the bar could cause the velocity distribution in the vicinity of the 2:1 outer Lindblad resonance (OLR) to become bimodal, due to the coexistence of orbits elongated along and perpendicular to the bars major axis. Today, we know that this mechanism does account for the Hercules stream (Dehnen 2000) as well as for some low-velocity streams such as the Pleiades (Minchev et al. 2010a). Quillen & Minchev (2005) also showed that the 4:1 ultra-harmonic (or second order) ILR of a 2-armed spiral structure* splits the velocity distribution into two features corresponding to two orbital families, one of them consistent with the Hyades. Test-particle simulations of a stellar disk consistent with the Milky Way kinematics, perturbed by a 2-armed spiral pattern (simulation parameters can be found in Minchev & Quillen 2007) showed that we could indeed reproduce the position of the Hyades stream in velocity-space only when the Sun is near the 4:1 ILR. The beauty of this simulation is that, while reproducing the Hyades stream, the other orbital family creates another remarkable feature in velocity space around $(U, V) \approx (10, 0)$ km/s, which is consistent with the Sirius stream (see Fig. 1, right panel). In order to reproduce the observed streams, the Sun should thus be at the same time close to the 2:1 OLR of the bar and 4:1 ILR of the spiral pattern. Since it has long been known that in the case of resonance overlap the last KAM surface between the two resonances is destroyed, resulting in chaotic behaviour, we expect that such a resonance overlap could give rise to radial migration of stars in the disk.

[1] Observatoire Astronomique, Université de Strasbourg, CNRS UMR 7550, F-67000 Strasbourg, France

[2] Astrophysikalisches Institut Potsdam, An der Sterwarte 16, D-14482 Potsdam, Germany

*Observations indicate that the Milky Way has a 4-armed structure, but with 2 more prominent arms
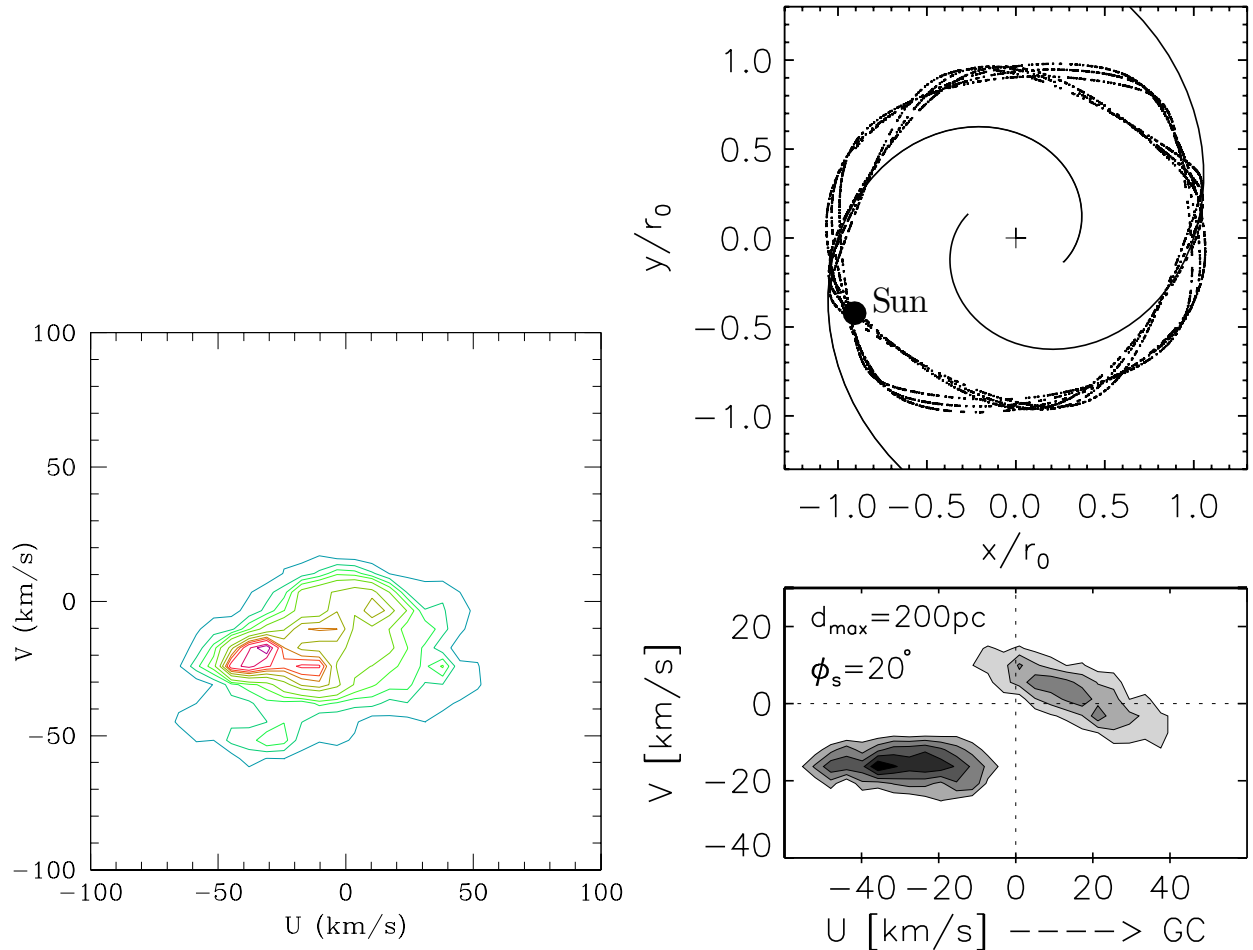
Fig. 1. Left Panel – Isocontours for the Geneva-Copenhagen survey (see Famaey et al. 2007) in the UV-plane (U is the velocity w.r.t. to the Sun in the direction of the Galactic center and V in the direction of Galactic rotation): the contours correspond respectively to 0.5, 0.8, 1.2, 1.5, 1.9, 2.6, 3.1, 3.5, 3.8, 4.2, 4.7, 5. stars/(km/s)^2. The Hyades stream, at $U \simeq -40$ km/s and $V \simeq -20$ km/s, and the Sirius stream at $U \simeq 10$ km/s and $V \simeq 0$ km/s are prominent features. The Pleiades stream is also visible at $U \simeq -15$ km/s and $V \simeq -20$ km/s, and the Hercules stream at $V \simeq -50$ km/s. **Top Right panel** – The effect of a 2-armed spiral structure on orbits near the 4:1 ILR. Note the splitting into 2 families of closed orbits in the frame moving with the (trailing) spiral pattern. For a Sun orientation at 20° with respect to a concave arm, both orbital families enter the solar neighborhood stellar velocity distribution (black filled circle). The galactocentric axes are in units of r_0 (the galactocentric radius of the Sun). **Bottom Right panel** – The effect on the UV-plane for the configuration shown in the top panel (selecting test particles in a 200 pc circle around the Sun). Each orbital family gives rise to a stream in velocity space. We can associate the dense clump at $(U, V) \approx (-40, -20)$ km/s with the Hyades and the shallow one at $(U, V) \approx (10, 0)$ km/s with Sirius.

3   Stellar migration

We have subsequently shown (Minchev & Famaey 2010) that a strong exchange of angular momentum indeed occurs when a stellar disk is perturbed by a central bar and spiral structure simultaneously (see Fig. 2). By using test-particle simulations, we confirmed that this effect was due to the overlap of first and second order resonances of each perturber, and showed that the mechanism was efficient throughout the whole disk, as such overlaps happen evrywhere. Beforehand, it was believed that radial mixing was solely caused by transient spirals (Sellwood & Binney 2002). The efficiency of the new spiral-bar mechanism was confirmed in fully self-consistent, Tree-SPH simulations, as well as high-resolution pure N-body simulations (Minchev et al. 2010b, see Fig. 3).
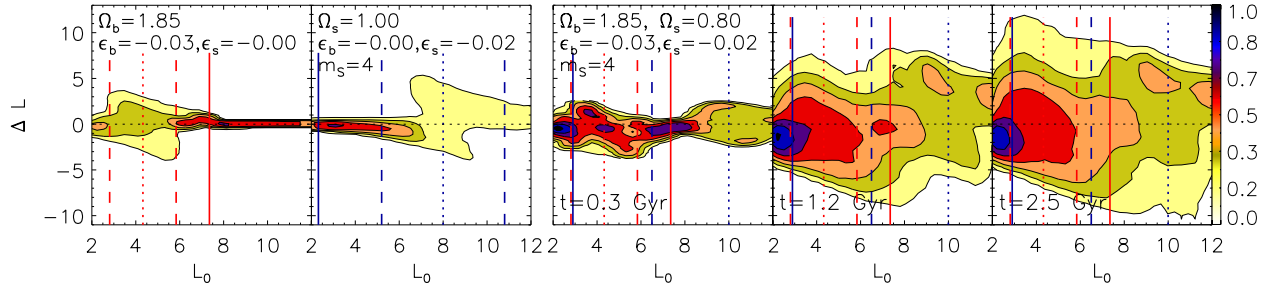
Fig. 2. Changes in the (vertical component of the) angular momentum, ΔL, as a function of the initial angular momentum, L_0. From left to right the first 2 panels show the effect of a bar or a spiral only, respectively, with parameters consistent with the Milky Way. The simultaneous propagation of the same perturbers is shown in the following 3 panels for $t = 0.3 - 2.5$ Gyr. The dotted lines show the corotation radii. The 2:1 and 4:1 LRs are indicated by the solid and dashed lines respectively (bar=red, spiral=blue). Figure is from Minchev & Famaey (2010).
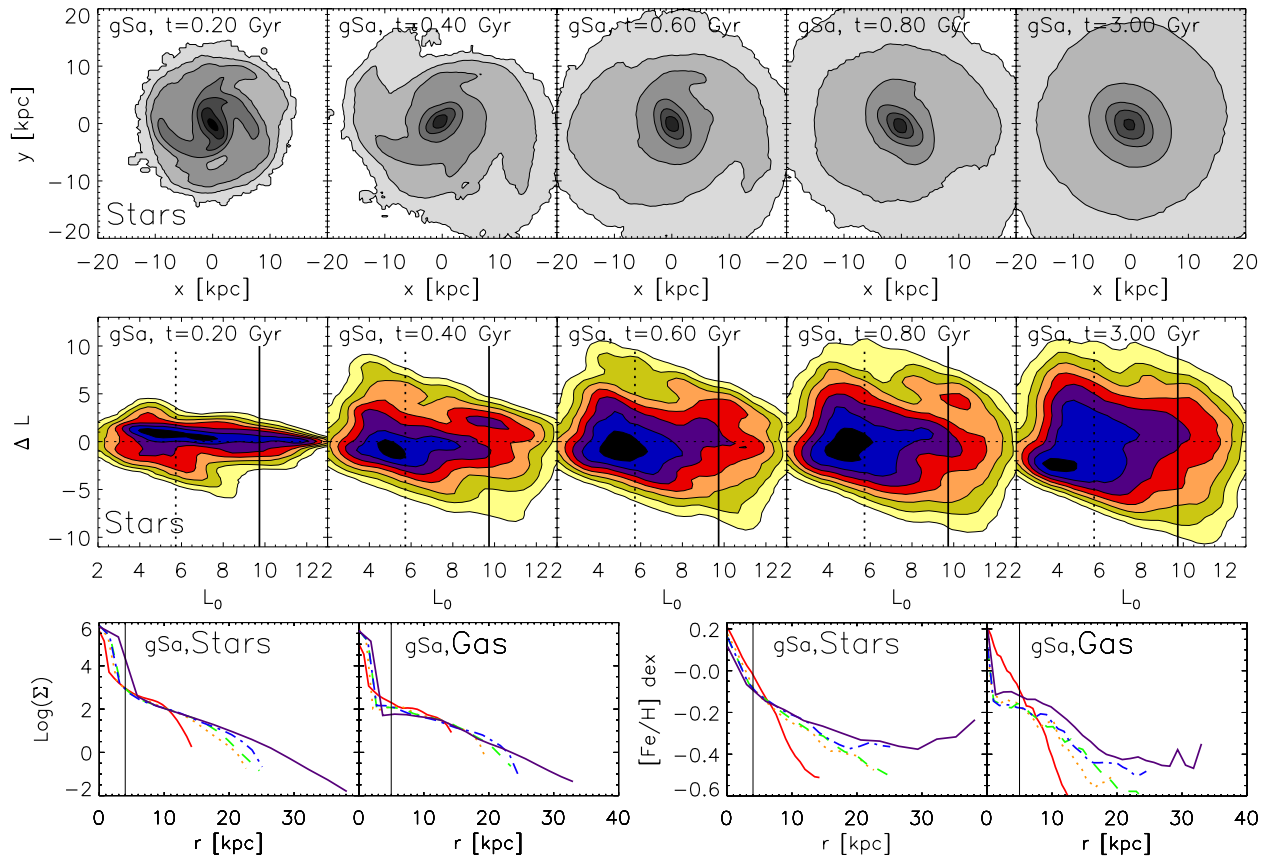
Fig. 3. Results of a Tree-SPH simulation, studying the exchange of angular momentum due to resonance overlap of bar and spiral. **Top row:** Time development of the stellar disk density contours of a giant Sa galaxy. **Second row:** ΔL as a function of the initial angular momentum, L_0. **Bottom row:** The evolution of the radial profiles of surface density (left) and metallicity (right) for the stellar and gaseous disks. The initial disk scale-lengths are indicated by the solid lines. The 5 time steps shown are as in the top row, indicated by solid red, dotted orange, dashed green, dotted-dash blue and solid purple, respectively, from Minchev et al. (2010b).

4   Conclusions

In order to reproduce the local velocity distribution of stars, the Sun should lie close to inner and outer Lindblad resonances of the spiral and bar, respectively. We showed that such a resonance overlap leads to radial migration

of stars. This happens throughout the whole disk, as other resonances do overlap too (see Fig. 2). This new theoretical mechanism for stellar migrations could be up to an order of magnitude more effective than the transient spirals mechanism. This effect is non-linear, strongly dependent on the strengths of the perturbers. The signature of this mechanism is a bimodality in the changes of angular momentum in the disk with maxima near the bar's corotation and its outer Lindblad resonance (Figs. 2 and 3). This is true regardless of the spiral pattern speed. This migration mechanism can create extended disks in both Milky Way-mass (Fig. 2) and low-mass galaxies, such as NGC 300 and M33, and it could also be responsible for the formation of a thick disk component early on in the galaxy evolution (Minchev et al., in preparation, see also Schoenrich & Binney 2009). However, important constraints on the mechanism come from the fact that it heats the disk too, and should not overheat it as compared to what is observed. We finally note that the most promising technique to put constraints on this mechanism in the Milky Way is "chemical tagging" (e.g., Bland-Hawthorn et al. 2010) which will become possible with the forthcoming spectroscopic survey HERMES, coupled with the precise astrometric measurements from GAIA.

References

Bland-Hawthorn J., et al., 2010, ApJ, 713, 166

Dehnen W., 2000, AJ, 119, 800

Famaey B., et al., 2005, A&A, 430, 165

Famaey B., et al., 2007, A&A, 461, 957

Famaey B., et al., 2008, A&A, 483, 453

Kalnajs A., 1991, in Sundelius B., ed., Dynamics of Disc Galaxies, Goteborgs Univ., p.323

Minchev I., Quillen A., 2007, MNRAS, 377, 1163

Minchev I., Famaey B., 2010, ApJ, 722, 112

Minchev I., et al., 2010a, MNRAS, 407, 2122

Minchev I., et al., 2010b, arXiv:1006.0484

Quillen A., Minchev I., 2005, AJ, 130, 576

Schoenrich R., Binney J., 2009, MNRAS, 399, 1145

Sellwood J., Binney J., 2002, MNRAS, 336, 785

Atelier commun A.S. Gaia - PNCG

Populations stellaires et modélisation de la Galaxie : maintenant et après Gaia, observations complémentaires au sol

SF2A 2010

24 juin 2010

Posters

- **L. Chemin et al.** : The catalogue of Radial Velocity standard stars for the RVS : status and progress

- **B. Giovannoli et al.** : LIRGs at intermediate redshift

- **B. Roukema** : Galactic Plane image sharpness as a check on cosmic microwave background mapmaking

- **S. Verley et al.** : The Herschel view of HII regions in M33 (HERM33ES)

THE CATALOG OF RADIAL VELOCITY STANDARD STARS FOR THE GAIA RVS: STATUS AND PROGRESS OF THE OBSERVATIONS

L. Chemin[1], C. Soubiran[1], F. Crifo[2], G. Jasniewicz[3], L. Veltz[4], D. Hestroffer[5], S. Udry[6], J. Berthier[5], A. Vigneron[5], D. Katz[2] and A. Siebert[7]

Abstract. A new full-sky catalog of Radial Velocity standard stars is being built for the determination of the Radial Velocity Zero Point of the RVS on board of Gaia. After a careful selection of 1420 candidates matching well defined criteria, we are now observing all of them to verify that they are stable enough over several years to be qualified as reference stars. We present the status of this long-term observing programme on three spectrographs : SOPHIE, NARVAL and CORALIE, complemented by the ELODIE and HARPS archives. Because each instrument has its own zero-point, we observe intensively IAU RV standards and asteroids to homogenize the radial velocity measurements. We can already estimate that 8% of the candidates have to be rejected because of variations larger than the requested level of 300 m s^{-1}.

Keywords: Gaia, Milky Way, stars, asteroids, radial velocity, high-resolution spectroscopy

1 Introduction

The purpose of this new spectroscopic catalog of standard stars is to calibrate the future radial velocities measured by the Radial Velocity Spectrometer (RVS) on board of the Gaia satellite (see e.g. Jasniewicz et al. 2010, and references therein). We refer to Crifo et al. (2009, 2010) for a complete description of the selection criteria and of the ground observations of the 1420 candidates as reference stars.

2 Status of the observations

A total of 4035 measurements is currently available for 1330 stars. It consists in new and archived observations performed with the NARVAL (98 measurements), CORALIE (688), SOPHIE (902), ELODIE (1057) and HARPS (1290) high-resolution spectrographs. Figure 1 (left panel) represents the spatial distribution in the equatorial frame of the number of measurements already obtained for the 1420 candidates. The majority of stars still lacking observations is located in the Southern part of the sky, because the Southern programme on CORALIE started later. In the North ($\delta > -15°$), $\sim$200 stars still lack a second measurement. The Northern programme should be completed in 2011.

3 Preliminary results

- ***Radial velocities of stars:*** We have first compared the radial velocities of 320 stars we have in common with Nidever et al. (2002). A mean difference of -40 m s^{-1} exists between both studies. This illustrates the zero-point issue that has to be solved for the calibration of the RVS (Jasniewicz et al. 2010). Among

---

[1] Laboratoire d'Astrophysique de Bordeaux, UMR 5804 (CNRS, Université Bordeaux 1), 33271 Floirac Cedex, France

[2] Observatoire de Paris, GEPI, UMR 8111 (CNRS , Université Denis Diderot Paris 7), 92195 Meudon, France

[3] GRAAL, UMR5024, (CNRS, Université Montpellier 2), 34095 Montpellier Cedex 05, France

[4] Astrophysikalisches Institut Potsdam, Potsdam, An der Sternwarte 16, D-14482 Potsdam, Germany

[5] Observatoire de Paris, IMCCE, UMR8028 (CNRS, Université Pierre & Marie Curie Paris 6), 75014, Paris, France

[6] Observatoire de Genève, 51 Ch. des Maillettes, 1290 Sauverny, Switzerland

[7] Observatoire Astronomique de Strasbourg, UMR 7550 (CNRS, Université de Strasbourg), 67000, Strasbourg, France
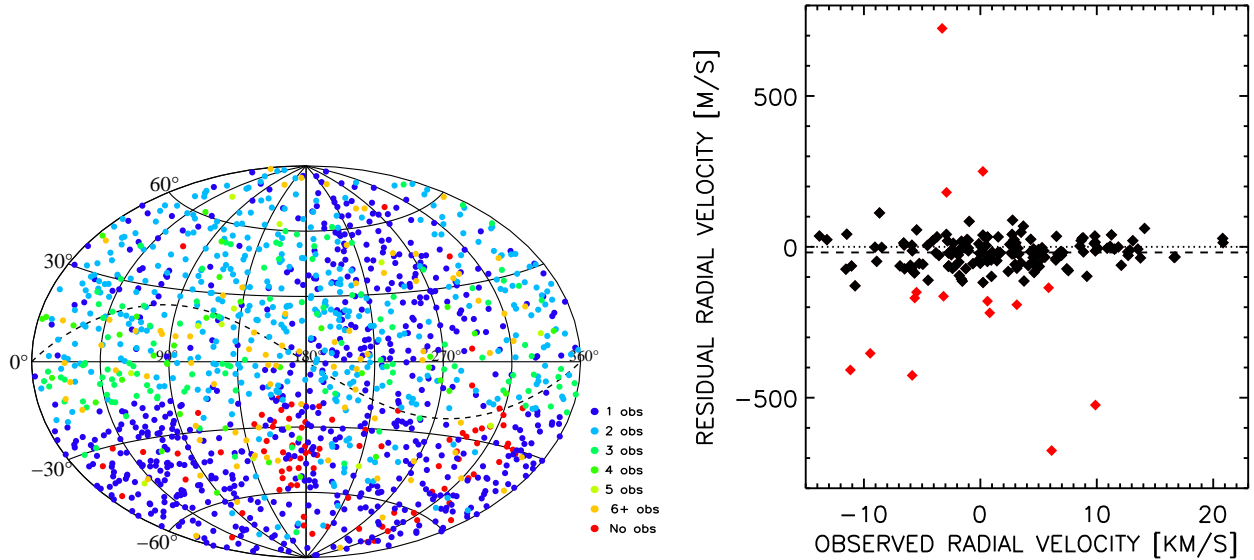
Fig. 1. *Left panel:* Number of ground-based observations of Gaia-RVS reference stars performed as of June 2010. The ecliptic is shown as a dashed line. *Right panel:* Residual velocities (observed - theoretical) for asteroids as a function of their observed velocities. The red dots deviate by more than 3σ.

those 320 stars 27 objects deviate by more than $\sim$300 m s^{-1}. Such a discrepancy between both studies may be due to variable stars that should not be considered as standard objects in a future analysis.

We have also done a preliminary statistical analysis our catalog. When selecting a sub-sample of 673 candidates for which at least two measurements have been performed it is seen that the velocity for $\sim$72% of them does not vary by more than 100 m s^{-1} during a time baseline of 0.5-2 years. Such a stability of radial velocities is very important to get the most accurate calibration of the RVS. The time variability of the catalog will be studied during the whole lifetime of the Gaia mission. Notice that $\sim$8% of the 673 stars exhibit a velocity variation of more than 300 m s^{-1}. Those objects likely correspond to variable stars.

- **Radial velocities of asteroids:** Observations of asteroids are very important for this project because they will allow the derivation of the zero point of the radial velocities for all reference sources. 171 measurements of 70 asteroids have been performed until now with SOPHIE. Their velocities have been compared with the theoretical values (Fig. 1, right panel) which have been derived using the MIRIADE webservice of the virtual observatory at IMCCE. The scatter of the residual (observed minus calculated) velocity is $\sigma \sim 45$ m s^{-1}. Points that are more deviant than 3σ (red symbols) correspond all to low signal-to-noise observations due to bad transparency conditions, or to badly derived velocity centroids due to e.g. double peaks in the cross-correlation function (observing conditions, contamination by the moon, ...). We are currently investigating the correlations of the observed and computed velocities with the physical properties of the asteroids (diameter, shape, rotation, phase, etc).

References

Crifo F., Jasniewicz G., Soubiran C., et al., 2009, SF2A 2009 conference proceedings, 267

Crifo F., Jasniewicz G., Soubiran C., et al., 2010, A&A, accepted, in press

Jasniewicz G., Crifo F., Soubiran C., et al., 2010, ELSA 2010 conference proceedings, in press

Nidever D. L., Marcy G. W., Butler R. P., Fischer D. A., Vogt S. S., 2002, ApJS, 141, 503

POPULATION SYNTHESIS MODELLING OF LUMINOUS INFRARED GALAXIES AT INTERMEDIATE REDSHIFT

E. Giovannoli[1], V. Buat[1], S. Noll[2], D. Burgarella[1] and B. Magnelli[3]

Abstract. Luminous InfraRed Galaxies (LIRGs) are particularly important for studying the build-up of the stellar mass from z=1 to z=0, and for determining physical properties of these objects at redshift 0.7. The global star formation rate (SFR) at $z \sim 0.7$ is mainly produced by LIRGs. We perform a multiwavelength study of an LIRGs sample in the Extended Chandra Deep Field South at z=0.7, selected at 24 μm by MIPS onboard *Spitzer Space Telescope* and detected in 17 filters. Data go from the near-ultraviolet to the mid-infrared. We distinguish a subsample of galaxies detected at 70 μm, which we compare to the rest of the sample to investigate the relative importance of this wavelength in determining of the physical parameters.

Keywords: galaxies evolution, infrared, Bayesian analysis, stellar content, SED-fitting

1 Introduction

Luminous InfraRed Galaxies (LIRGs) are commonly defined as galaxies whose infrared (IR, 8-1000 μm) emission is higher than $10^{11} L_{\odot}$ and lower than $10^{12} L_{\odot}$. A z ~1 only 30% of LIRGs exhibit features linked to violent merging (Bell et al. 2007), (Zheng et al. 2007) : most of them look like bright spirals that experience a secular evolution without violent events. This morphological difference between local and distant LIRGs is corroborated by the analysis of their star formation rate (SFR). Whereas local LIRGs are experiencing a strong starburst, distant LIRGs do not seem to strongly depart from the mean SFR - stellar mass ($M_{\star}$) relation found at z=1 (Elbaz et al. 2007).

2 Analysis of a LIRGs sample

We apply a multiwavelength analysis from the far-ultraviolet (FUV) to the IR, based on SED (Spectral Energy Distribution)-fitting, on a sample of z=0.7 LIRGs selected at 24 μm (Giovannoli et al., 2010). Our aim is to study this galaxy sample, representative of LIRGs at intermediate redshift, in a very homogeneous and systematic way to determine the main characteristics of their stellar populations and dust emission. We study LIRGs with the SED-fitting code CIGALE (Code Investigating GALaxy Emission * : Noll et al. 2009b, Burgarella et al. 2005), which provides an estimation of physical parameters of galaxies thanks to a Bayesian-like analysis. The stellar populations synthesis code of Maraston et al. (2005) is adopted to model the stellar emission (UV, optical, and NIR wavelengths). The created stellar population spectra are then attenuated by using a synthetic Calzetti-based attenuation law (Calzetti et al. 2000) before adding the dust emission as given by the infrared SED library (semi-empirical one-parameter models of Dale & Helou (2002)).

Figure 1 shows distributions for the parameters related to the star formation history and the attenuation ($M_{\star}$, infrared luminosity L_{dust}, SFR, attenuation in the V-band A_V, fraction in mass of the young stellar population f_{ySP}, and fraction of AGN f_{AGN}) calculated with the Bayesian-like analysis in CIGALE, for the subsample detected at 70 μm and for the whole sample. The masses found for the 70 μm sample are shifted towards higher masses then in the total sample. We observe a similiar situation for L_{dust} and the SFR; the values are in the range [10^{11} ; 10^{12}] $L_{\odot}$ and [10 ; 92] $M_{\odot}.yr^{-1}$, respectively, with mean values higher than ones found for the total sample. This shift is expected because of the 70 μm detection limit

[1] Laboratoire d'Astrophysique de Marseille, OAMP, Université Aix-Marseille, CNRS, 38 rue Frédéric Joliot-Curie, 13388 Marseille cedex 13, France

[2] Institut für Astro- und Teilchenphysik, Universität Innsbruck, Technikerstr. 25/8, 6020 Innsbruck, Austria

[3] Max-Planck-Institut für Extraterrestrische Physik (MPE), Postfach 1312, 85741 Garching, Germany.

*Web address to use CIGALE : http://www.oamp.fr/cigale/
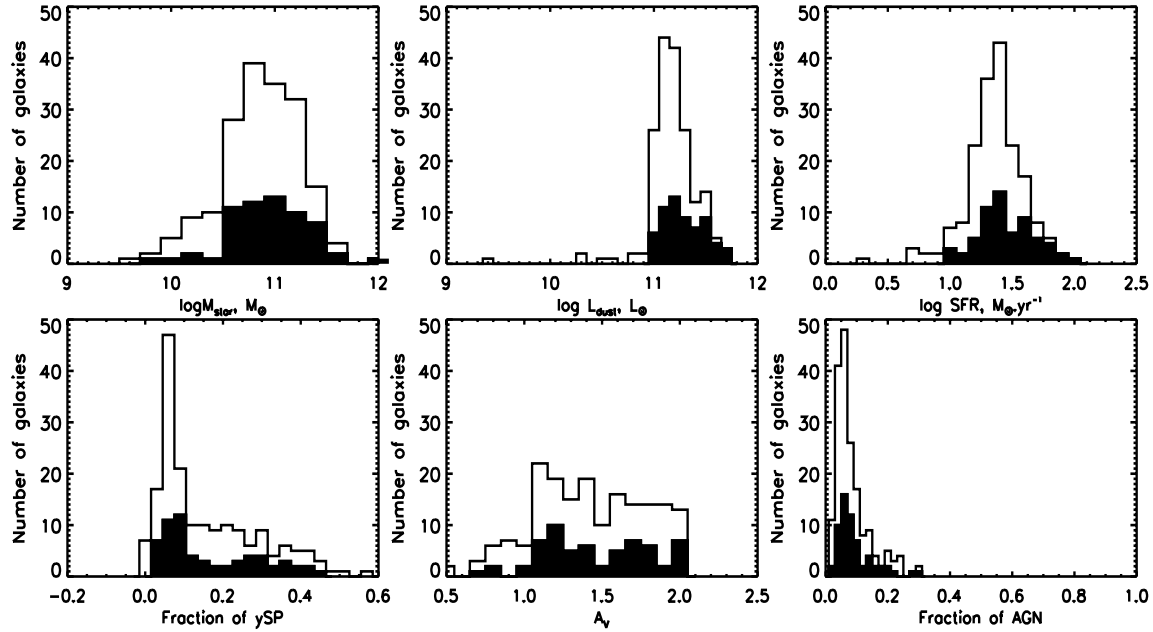
Fig. 1. Bayesian results of the code for the following parameters : $M_\star$, L_{dust}, SFR, A_V, f_{ySP}, f_{AGN}. The empty histogram represents the total sample and the full one represents the 70 μm sample.

(2.7 mJy at 5σ): at this wavelength, we only detect luminous and massive galaxies. The distribution of f_{ySP} is broad with a long tail towards high values, and A_V lies between 0.5 and 2.1 mag with very few objects under 1.0 mag and quite a homogeneous distribution between 1.0 and 2.0.

Galaxies in the total sample have $M_\star$ between 10^{10} and 10^{12} M$_\odot$ with a peak at $10^{10.8}$M$_\odot$. We find the SFR between 3 and 92 M$_\odot$yr^{-1} with a peak at 23 M$_\odot$yr^{-1}. For f_{ySP} and A_V, we observe the same distribution as for the 70 μm sample. For both samples, f_{AGN} is relatively low, between 0.0 and 0.3 with the majority of the objects in the interval [0;0.1]. We consider that there is a definite contamination of L_{dust} by an AGN when $f_{AGN} > 15\%$, because a contamination lower than15% does not significantly modify the total IR emission.

3   Conclusions

We fit the SEDs of our sample of LIRGs with the CIGALE code, which combines stellar and dust emissions in a physical way. This study is the first use of CIGALE at a redshift higher than 0. The multiwavelength data analysis performed in this study provides reliable estimates of several physical parameters based on a Bayesian-like analysis.

References

Bell, E. F., Zheng, X. Z, Papovich, C. et al., 2007, ApJ, 663, 834

Buat, V., Takeuchi, T. T., Iglesias-Páramo, J, et al. 2007, ApJS, 173, 404

Buat, V., Boissier, S., Burgarella, D., et al. 2008, A&A, 483, 107

Burgarella, D., Buat, V. & Iglesias-Páramo, J. 2005, MNRAS, 1413,1425

Calzetti, D., Armus, L., Bohlin, R. C., et al. 2000, 533, 682

Dale, D. & Helou, G. 2002, ApJ, 576,159

Elbaz, D., Daddi, E., Le Borgne, et al., 2007, A&A ,468, 33

Giovannoli, E., Buat, V., Noll., S., Burgarella, D., Magnelli, B., 2010, arXiv,1006,5555

Maraston, C., 2005, MNRAS, 362, 799

Noll, S., Burgarella., D., Giovannoli, E., et al., 2009, A&A, 507, 1793

Zheng, X. Z., Dole, H., Bell, E. F., et al, 2007, ApJ, 670, 301

GALACTIC PLANE IMAGE SHARPNESS AS A CHECK ON COSMIC MICROWAVE BACKGROUND MAPMAKING

B. F. Roukema[1]

Abstract. The largest uncollapsed inhomogeneity in the observable Universe is statistically represented in the quadrupole signal of the cosmic microwave background (CMB) sky maps as observed by the Wilkinson Microwave Anisotropy Probe (WMAP). The constant temporal offset of -25.6 ms between the timestamps of the spacecraft attitude and observational data records in the time-ordered data (TOD) of the WMAP observations was suspected to imply that previously derived all-sky CMB maps are erroneous, and that the quadrupole is in large part an artefact. The optimal focussing of bright objects in the Galactic Plane plays a key role in showing that no error occurred at the step of mapmaking from the calibrated TOD. Instead, the error had an effect when the uncalibrated TOD were calibrated. Estimates of the high-latitude quadrupole based on the wrongly calibrated WMAP maps are overestimated by about 15–60%.

Keywords: cosmic background radiation, galaxy: center, galaxy: disk, techniques: image processing

Although the primary aim of cosmic microwave background (CMB) all-sky observation missions is cosmological, the Galaxy constitutes a major component of the resulting data set. Liu & Li (2010) reconstituted all-sky maps from Wilkinson Microwave Anisotropy Probe (WMAP, Bennett et al. 2003) time-ordered data (TOD) and suggested that the quadrupole present in the official versions of the maps is mostly an artefact, since their own maps had a weaker quadrupole. They later traced this to a timing offset of -25.6 ms between the timestamps of the spacecraft attitude and observational data records in the calibrated TOD files (Liu et al. 2010). Since the offset is also present in the uncalibrated TOD files, it could have affected either (i) the calibration step or (ii) the mapmaking step.

The WMAP 3-year calibrated TOD were compiled into maps using Liu et al. (2010)'s publicly available data analysis pipeline[*], and patched for using the GNU Data Language (GDL) and for two different timing error tests. In both cases, the timing offset, written as a multiple δt of an exposure time in a given waveband, where $\delta t = 0.5$ corresponds to the timing offset used by the WMAP collaboration, was varied in order to detect its effect on a relevant statistic of the maps. Testing an error at step (i) was done by creating low-resolution maps and finding the maps with the least variance per pixel (Roukema 2010b).[†] Testing an error at step (ii) was done by calculating high-resolution maps that included sub-cosmological objects, and finding the best focussed maps (Roukema 2010a).[‡] The results, summarised in Table 1, showed to very high significance that the error affected the calibration step, but did not affect the mapmaking step directly. However, maps made from the wrongly calibrated data necessarily include the calibration error. For example, estimates of the high-latitude quadrupole based on the wrongly calibrated WMAP maps are overestimated by about 15–60% (Roukema 2010b). Figures 1 and 2 illustrate the sharpest focus test.

References

Bennett, C. L., Halpern, M., Hinshaw, G., et al. 2003, ApJSupp, 148, 1, [arXiv:astro-ph/0302207]

Liu, H., & Li, T. 2010, ArXiv e-prints, [arXiv:0907.2731]

Liu, H., Xiong, S., & Li, T. 2010, ArXiv e-prints, [arXiv:1003.1073]

Roukema, B. F. 2010a, A&A, 518, A34, [arXiv:1004.4506]

Roukema, B. F. 2010b, A&A, submitted, [arXiv:1007.5307]

---

[1] Toruń Centre for Astronomy, Nicolaus Copernicus University, ul. Gagarina 11, 87-100 Toruń, Poland

[*] http://cosmocoffee.info/viewtopic.php?p=4525, http://dpc.aire.org.cn/data/wmap/09072731/release_v1/source_code/v1/

[†] http://cosmo.torun.pl/GPLdownload/LLmapmaking_GDLpatches/LLmapmaking_GDLpatches_0.0.4.tbz

[‡] http://cosmo.torun.pl/GPLdownload/LLmapmaking_GDLpatches/LLmapmaking_GDLpatches_0.0.3.tbz
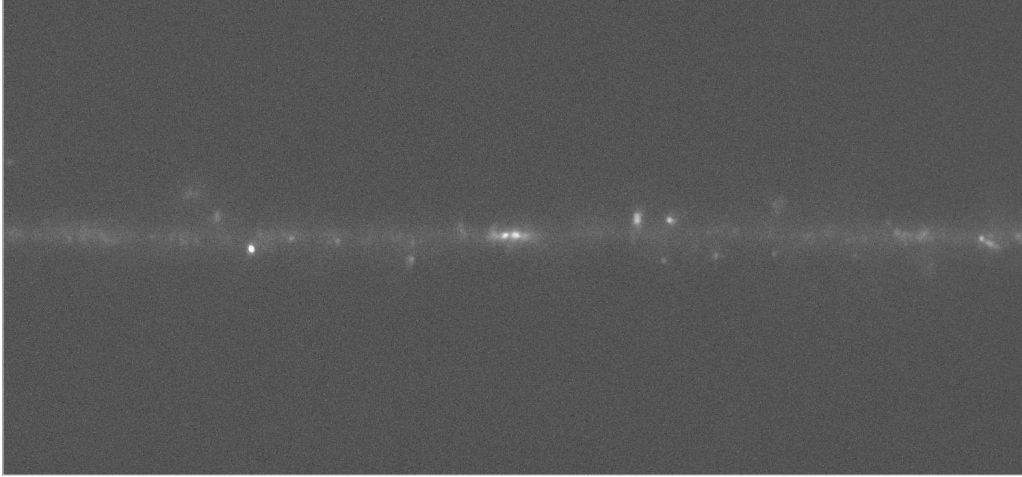
Fig. 1. Correctly focussed ($\delta t = 0.5$, Roukema 2010a) but wrongly calibrated (Roukema 2010b) WMAP W band (94 GHz) image of the $53.0° \times 24.7°$ region centred at the Galactic Centre (North up, East left), after monopole and dipole subtraction, on a grey scale ranging from black (-20 mK) to white (+40 mK). To zoom in, see Fig. 4, Roukema (2010a).

Table 1. Comparison of sharpest focus and minimum variance methods of testing for a timing offset error.

short name	minimum variance	sharpest focus
reference	Roukema (2010b)	Roukema (2010a)
step to understand	uncal. TOD $\rightarrow$ cal. TOD	cal. TOD $\rightarrow$ map
step analysed	cal. TOD $\rightarrow$ map	cal. TOD $\rightarrow$ map
planets & Gal. Plane	excluded	included
N_{side}	8	2048
statistic	variance per pixel	brightness of 503-rd brightest pixel
max/min	min	max
rejected hypothesis	$\delta t = 0.5$ rejected at 8.5σ	$\delta t = 0$ rejected at 4.6σ
accepted hypothesis	$(\delta t - 0.5) \times 52.1$ ms $= -25.6$ ms	$\delta t = 0.5$
conclusion	calibration step wrong	mapmaking step right

Fig. 2. Wrongly focussed, wrongly calibrated WMAP W band image, as for Fig. 1, with a timing offset $\delta t = -5$, i.e. exaggerated by a factor of ten beyond that which generated the calibration error. To zoom in, see Fig. 2, Roukema (2010a).

THE HERSCHEL VIEW OF HII REGIONS IN M 33 (HERM33ES)

S. Verley[1], M. Relaño[1], C. Kramer[2], E.M. Xilouris[3], M. Boquien[4], D. Calzetti[4], F. Combes[5], C. Buchbender[2], J. Braine[6], G. Quintana-Lacaci[2], F.S. Tabatabaei[7], S. Lord[8], F. Israel[9], G. Stacey[10] and P. van der Werf[9]

Abstract. Within the framework of the HERM33ES Key Project (Kramer et al. 2010), using the high resolution and sensitivity of the Herschel photometric data, we study the compact emission in the Local Group spiral galaxy M 33. We present a catalogue of 159 compact emission sources in M 33 identified by SExtractor in the 250 μm SPIRE band which is the one that provides the best spatial resolution. We measure fluxes at 24 μm and Hα for those 159 extracted sources. We find a very strong Pearson correlation coefficient with the MIPS 24 μm emission ($r_{24} = 0.94$) and a rather strong correlation with the Hα emission, although with more scatter ($r_{H\alpha} = 0.83$). Due to the very strong link between the 250 μm compact emission and the 24 μm and Hα emissions, by recovering the star formation rate from standard recipes for HII regions, we are able to provide star formation rate calibrations based on the 250 μm compact emission alone. Finally, the morphological study of a set of three Hα shells shows that there is a displacement between far-ultraviolet and the SPIRE bands, while the Hα structure is in general much more coincident with the cool dust.

Keywords: galaxies: individual: M 33, galaxies: ISM, local group, galaxies: spiral

1 SPIRE 250 μm calibration of the star formation rate for HII regions in M 33

In order to create a catalogue of compact emission sources in the SPIRE 250 μm band, we use the SExtractor software (Bertin & Arnouts 1996). The photometry of the 159 extracted sources is computed using the parameter FLUX_ISO given by SExtractor, which uses isophotal photometry (sum of all the pixels above a threshold given by the lowest isophot: 16 times the background r.m.s.). Since most of the extracted objects are along the spiral pattern of the galaxy, we believe many of the sources may be directly linked to star formation (SF). This suggests that the SPIRE 250 μm compact emission could be a reliable SF tracer in the vicinity of HII regions. Therefore, we concentrate our preliminary work on the 250 μm compact emission and compare its properties with standard SF tracers such as the Hα emission line and the 24 μm compact emission linked to HII regions (Calzetti et al. 2005, 2007, 2010; Verley et al. 2009, 2010a). To recover the Hα+24 μm SF rate (SFR), our best fit leads to:

$$\text{SFR } [\text{M}_\odot \text{ yr}^{-1}] = 8.71 \times 10^{-45} L(250 \,\mu\text{m})^{1.03} \quad , \tag{1.1}$$

where $L(250 \,\mu\text{m})$ is in erg s^{-1}. To recover the SFR(24), we need the following calibration:

$$\text{SFR } [\text{M}_\odot \text{ yr}^{-1}] = 3.47 \times 10^{-44} L(250 \,\mu\text{m})^{1.02} \quad , \tag{1.2}$$

also with $L(250 \,\mu\text{m})$ in erg s^{-1}. The uncertainties are 0.04 and 0.03 for the exponents in Eqs. 1.1 and 1.2, respectively, while the calibration constants have uncertainties of 4.0 and 2.7%, respectively. Please, see Verley et al. (2010b) for more information.

---

[1] Dept. Física Teórica y del Cosmos, Universidad de Granada, Spain

[2] Instituto Radioastronomia Milimetrica (IRAM), Av. Divina Pastora 7, Nucleo Central, E-18012 Granada, Spain

[3] Institute of Astronomy and Astrophysics, National Observatory of Athens, P. Penteli, 15236 Athens, Greece

[4] Department of Astronomy, University of Massachusetts, Amherst, MA 01003, USA

[5] Observatoire de Paris, LERMA, 61 Av. de l'Observatoire, 75014 Paris, France

[6] Lab. d'Astrophysique, Université 1 et Observatoire de Bordeaux, OASU, UMR 5804, CNRS/INSU, Floirac F-33270, France

[7] Max-Planck-Institut für Radioastronomie (MPIfR), Auf dem Hügel 69, D-53121 Bonn, Germany

[8] Infrared Processing and Analysis Center, MS 100-22 California Institute of Technology, Pasadena, CA 91125, USA

[9] Leiden Observatory, Leiden University, PO Box 9513, NL 2300 RA Leiden, The Netherlands

[10] Department of Astronomy, Cornell University, Ithaca, NY 14853, USA
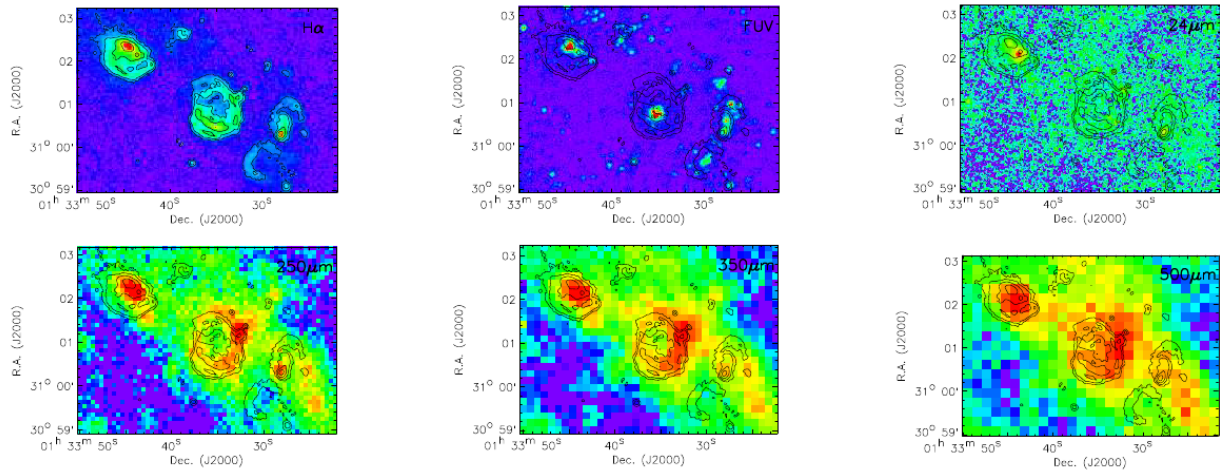
Fig. 1. Continuum-subtracted Hα image of a set of large shells in the outer north part of M 33 (top left). Contours are overlaid in this image to better enhance the shell features (levels are at 20, 49, 122, 300 of Hα emission measure) and repeated in the other images for comparison.

2   SPIRE emission distributions for HII regions

Taking advantage of the unprecedented Herschel resolution at the SPIRE wavelength bands, we also focus on a more precise study of some striking Hα shells in the northern part of the galaxy (see Fig. 1). The morphological study of the Hα shells shows a displacement between far-ultraviolet, Hα, and the SPIRE bands. The different locations of the Hα and far-ultraviolet emissions with respect to the SPIRE cool dust emission leads to a dynamical age of a few Myr for the Hα shells and the associated cool dust (Relaño & Beckman 2005).

We refer the reader to Kramer et al. (2010); Braine et al. (2010); Boquien et al. (2010) for more details about the overall HERM33ES preliminary results, as well as for a first presentation of the PACS and SPIRE maps of the entire galaxy, together with spatially averaged spectral energy distributions.

References

Bertin, E. & Arnouts, S. 1996, A&AS, 117, 393

Boquien, M., Calzetti, D., Kramer, C., et al. 2010, A&A, 518, L70

Braine, J., Gratier, P., Kramer, C., et al. 2010, A&A, 518, L69

Calzetti, D., Kennicutt, R. C., Engelbracht, C. W., et al. 2007, ApJ, 666, 870

Calzetti, D., Kennicutt, Jr., R. C., Bianchi, L., et al. 2005, ApJ, 633, 871

Calzetti, D., Wu, S., Hong, S., et al. 2010, ApJ, 714, 1256

Kramer, C., Buchbender, C., Xilouris, E. M., et al. 2010, A&A, 518, L67

Relaño, M. & Beckman, J. E. 2005, A&A, 430, 911

Verley, S., Corbelli, E., Giovanardi, C., & Hunt, L. K. 2009, A&A, 493, 453

Verley, S., Corbelli, E., Giovanardi, C., & Hunt, L. K. 2010a, A&A, 510, A64

Verley, S., Relaño, M., Kramer, C., et al. 2010b, A&A, 518, L68